

Article

Structural and Electronic Properties of (TMTTF)₂X Salts with Tetrahedral Anions

Roland Rösslhuber [†], Eva Rose [†], Tomislav Ivek [‡], Andrej Pustogow, Thomas Breier, Michael Geiger, Karl Schrem, Gabriele Untereiner and Martin Dressel * 

1. Physikalisches Institut, Universität Stuttgart, Pfaffenwaldring 57, D-70569 Stuttgart, Germany; roland.roesslhuber@pi1.physik.uni-stuttgart.de (R.R.); eva.rose@pi1.physik.uni-stuttgart.de (E.R.); tivek@ifs.hr (T.I.); andrej.pustogow@pi1.physik.uni-stuttgart.de (A.P.); acs@pi1.physik.uni-stuttgart.de (T.B.); m.geiger@fkf.mpg.de (M.G.); cienkowska-schmidt@pi1.physik.uni-stuttgart.de (K.S.); gabriele.untereiner@pi1.physik.uni-stuttgart.de (G.U.)

* Correspondence: dressel@pi1.physik.uni-stuttgart.de; Tel.: +49-711-685-64946

[†] These authors contributed equally to the work.

[‡] Permanent address: Institut za fiziku, Bijenička 46, HR-10000 Zagreb, Croatia.

Academic Editor: Helmut Cölfen

Received: 14 February 2018; Accepted: 28 February 2018; Published: 4 March 2018

Abstract: Comprehensive measurements of the pressure- and temperature-dependent dc-transport are combined with dielectric spectroscopy and structural considerations in order to elucidate the charge and anion orderings in the quasi-one-dimensional charge-transfer salts (TMTTF)₂X with non-centrosymmetric anions X = BF₄, ClO₄ and ReO₄. Upon applying hydrostatic pressure, the charge-order transition is suppressed in all three compounds, whereas the influence on the anion order clearly depends on the particular compound. A review of the structural properties paves the way for understanding the effect of the anions in their methyl cavities on the ordering. By determining the complex dielectric constant $\hat{\epsilon}(\omega, T)$ in different directions we obtain valuable information on the contribution of the anions to the dielectric properties. For (TMTTF)₂ClO₄ and (TMTTF)₂ReO₄, ϵ_b' exhibits an activated behavior of the relaxation time with activation energies similar to the gap measured in transport, indicating that the relaxation dynamics are determined by free charge carriers.

Keywords: Fabre salts; one-dimensional conductors; charge order; anion order; electronic transport; pressure dependence; dielectric spectroscopy

PACS: 71.30.+h, 74.70.Kn, 75.25.Dk, 71.27.+a, 72.15.-v, 77.22.Gm

1. Introduction

Electronic correlations play a decisive role in the quasi-one-dimensional molecular charge-transfer salts (TMTTF)₂X, where TMTTF means tetramethyltetrathiafulvalene. As a result of the 2:1 stoichiometry with positively charged (TMTTF)⁰⁺, $\rho_0 = 0.5$, and monovalent anions X⁻, the (TMTTF)₂X salts should have a 3/4-filled conduction band. The slight dimerization of the molecular stacks leads to a splitting into a completely filled lower and a half-filled upper band; accordingly, metallic properties are expected. This behavior is observed in the sibling TMTSF compounds, known as Bechgaard salts, here TMTSF stands for tetramethyltetraselenafulvalene. Due to the reduced dimension, Fermi liquid theory breaks down separating spin and charge degrees of freedom [1,2].

In the case of the Fabre-salts TMTTF, however, a minimum in resistivity $\rho(T)$ is observed at $T_\rho \approx 250$ K, followed by a strong increase at T_{CO} [3–5]. The first phase below T_ρ is referred to as charge localization or dimer Mott insulator, whereas the charge-order (CO) transition occurs at T_{CO} , usually somewhere below 160 K. Both states arise due to strong electronic correlations which are well described

by the extended Hubbard model taking into account on-site U and nearest-neighbor Coulomb interactions V [6]. Intense research over the last decades revealed a colorful interplay of charge, spin and lattice degrees of freedom and established a generic phase diagram. The temperature-pressure diagram is shown in Figure 1 and includes $(\text{TMTTF})_2X$ and $(\text{TMTSF})_2X$ salts with centrosymmetric anions $X = \text{Br}, \text{PF}_6, \text{AsF}_6, \text{SbF}_6, \text{TaF}_6$, wherein the position can be tuned either by external pressure or by substituting the anions, causing chemical pressure. In the phase diagram Figure 1, the compounds with non-centrosymmetric anions, such as $\text{SCN}, \text{FSO}_3, \text{NO}_3, \text{BF}_4, \text{ClO}_4$ and ReO_4 are missing, as they exhibit ordering of the anions upon cooling.

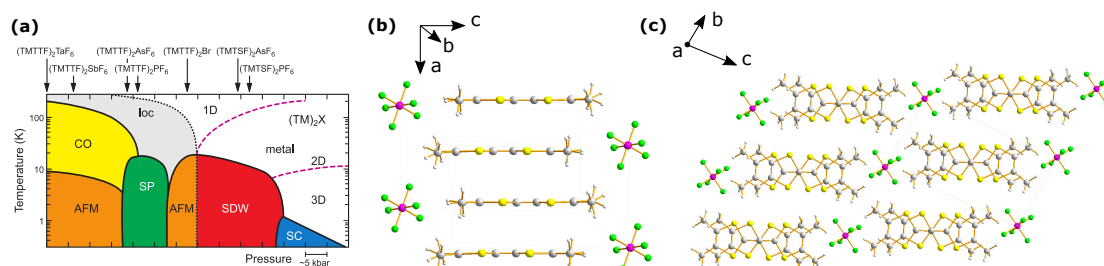


Figure 1. (a) The generic phase diagram of the tetramethyltetrathiafulvalene (TMTTF) and tetramethyltetraselenafulvalene (TMTSF) salts with centrosymmetric anions, as first suggested by Jérôme [7] and further refined by other groups [2]. The position can be tuned either by external physical pressure or by chemical pressure via substituting the anion. The arrows indicate the ambient pressure position of the particular compounds with different anions. Decreasing the anion size corresponds to increasing pressure upon which the properties become more metallic and less one-dimensional. The full and dashed lines indicate phase transitions and crossovers, respectively. The various terms are shortened as follows: CO charge order, loc charge localization, SP spin-Peierls, AFM antiferromagnet, SDW spin density wave and SC superconductivity; (b) Crystal structure of $(\text{TMTTF})_2\text{PF}_6$ [8] illustrating the stacking of the TMTTF molecules and the anions along the a -direction and, (c) in the bc -plane showing the separation of the TMTTF stacks by anions.

2. Structural Considerations

Before we report our experimental studies on the electronic properties of $(\text{TMTTF})_2X$ and discuss the temperature and pressure development, let us summarize the structural aspects known for this class of materials. As the best studied example, the crystal structure of $(\text{TMTTF})_2\text{PF}_6$ under ambient conditions [8] is exemplarily shown in Figure 1b and c for the $(\text{TMTTF})_2X$ salts. Commonly they exhibit a triclinic space group $P\bar{1}$ with inversion centers located in between the TMTTF molecules and on the anions [9–14]. Most importantly, the planar TMTTF molecules are arranged in zig-zag stacks along the a -direction (Figure 1b) giving rise to the quasi-one-dimensional physics in the Fabre salts [3]. The anions separate the TMTTF stacks along the $b + c$ direction (Figure 1c) and mediate the inter-stack coupling. Moreover, due to the presence of the anions, a slight dimerization is introduced on the TMTTF stacks which decreases upon cooling [15]. This already indicates that the counterions play a more complex role than just acting as spacers between the TMTTF stacks and that their symmetry affects the electronic properties [4,16–18].

The anions are located in cavities, which are constituted by the methyl end groups of the six nearest neighbor TMTTF molecules [19]. Depending on their size, symmetry, and polarizability, the anions and the methyl groups are slightly deformed, leading to a more or less snug fit in the cavities [14,16,17,20,21]. For that reason, the anions possess some limited rotational and translational degrees of freedom that are activated at higher temperatures [22,23]. The methyl groups basically form a centrosymmetric environment with symmetry axes close to the ones of the octahedral anions. This implies that for non-centrosymmetric entities, i.e., linear, triangular, tetrahedral anions, orientational disorder becomes an issue [17,24].

At lower temperatures—when thermal disorder is reduced—weak hydrogen-bonds are formed between the ligands of the counter ions and the closest methyl groups [25]. Moreover, there is a link between the S-atom of the nearest TMTTF molecule and the anion ligand O or F-atom [26], evidenced by an anion dependence of the sulfur to anion-ligand distance $d_{\text{AL-S}}$ [4,18] (Table 1). It is important to emphasize, that via the methyl groups any structural or charge modification in the TMTTF molecules influences the position of the anions and vice versa [17].

At elevated temperatures, the symmetry of the anions does not play a crucial role, for these entities are subject to rotation and disorder. Upon cooling, however, the motion is hindered and the anions get locked in certain positions, where the symmetry of the anions becomes an important aspect. The alternating orientation of the tetrahedra along and perpendicular to the stacks leads to a doubling of the lattice periodicity; hence the anion order is a structural transition with wave vector $q_{\text{AO}} = (\frac{1}{2}, \frac{1}{2}, \frac{1}{2})$. X-ray absorption near edge structure (XANES or NEXAFS) [27] and infrared optical spectroscopy [23] measurements unanimously identify a tetramerization of the TMTTF stacks at the AO transition T_{AO} , the latter also providing evidence for a 0110 charge pattern. A scheme of the corresponding modification of the structure and the charge pattern is shown in Figure 2e.

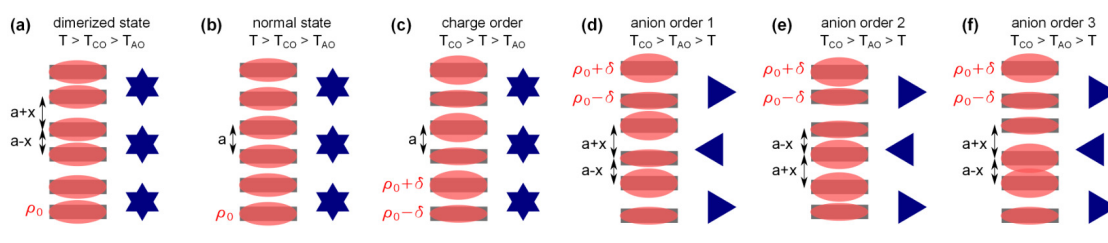


Figure 2. Sketch of the molecular and charge arrangements for different states of $(\text{TMTTF})_2\text{X}$ salts. The organic molecules are depicted as rectangles; the amount of charge ρ_0 , $\rho_0 \pm \delta$ is illustrated by red ellipses of different size. The anions are shown as blue hexagons or triangles, depending on the centrosymmetry. (a) The TMTTF stacks are dimerized at room temperature, $a \pm x$. The degree of dimerization decreases upon cooling, thus equalizing the TMTTF sites towards the uniform state in (b). Panel (c) illustrates how charge disproportionation develops as the charge-ordered state is entered with a 1010 charge pattern along the stacking direction. A priori, three different charge configurations are possible in the anion-ordered phase: (d) one with a 1010 pattern and (e,f) two with a 1100 pattern. Our optical studies [23] have revealed that the tetramerized state (e) forms due to the anion order, with an intra-dimer molecular distance $a - x$, and the dimers separated by $a + x'$ and $a + x''$.

In this respect, charge order as well as anion order in the $(\text{TMTTF})_2\text{X}$ salts still bear some mystery. Among the remaining questions are (i) about the exact mechanism for CO involving the anions, hence (ii) about the nature of interplay, if there is any, between CO and AO and (iii) about the role of polarizability of the anions for CO and AO.

2.1. Charge Order

Charge order is caused by redistribution of electronic charge within the TMTTF stack resulting in an alternating arrangement of differently charged molecules $(\text{TMTTF})^{+0.5+\delta}$ and $(\text{TMTTF})^{+0.5-\delta}$ along the a -direction. This charge disproportionation is observed in all TMTTF salts considered here, except $(\text{TMTTF})_2\text{ClO}_4$. Charge order lifts the inversion symmetry and conceptually doubles the unit cell. Halving the Brillouin zone leads to the opening of a gap in the electronic density of state [3]. The latter is observed as a strong increase of resistivity at T_{CO} [4,5] whereas the charge disproportionation is evidenced by nuclear magnetic resonance (NMR) [28,29], dielectric [30–36] and optical spectroscopy [23,37,38], as well as by synchrotron X-ray diffraction measurements [39]; the latter results evidence a 1010 charge pattern. The electrical transition proceeds continuously, wherein the charge disproportionation and the energy gap exhibit a temperature dependence that resembles

the mean-field behavior of a second-order phase transition [4,23]. An overview of the transition temperatures and structural parameters determined at room temperature is given in Table 1.

Figure 2 illustrates the molecular and charge arrangements for the different states realized in the $(\text{TMTTF})_2\text{X}$ salts. Panel a corresponds to the state at high temperatures, which exhibits a finite dimerization of the organic molecules. Upon cooling, the dimerization diminishes [15], approaching the arrangement shown in panel b. The charge disproportionation starts to develop upon entering the charge-ordered state with a 1010 pattern along the stacking direction as sketched in panel c.

2.2. Anion Contribution to Charge Order

From a general point of view, the $(\text{TMTTF})_2\text{X}$ salts are stabilized by the charge transfer of half an electron from the TMTTF molecules to the anions. Therefore it seems reasonable that charge redistribution at the CO transition introduces structural modifications [17]. Nevertheless, the associated alternation in the crystal structure could not be resolved for a long time [15,40], and as a result, the charge order transition was first considered as a “structureless transition” of unknown origin [41]. Only recent ^{19}F -NMR studies [42], measurements of the thermal expansion [43,44], neutron scattering [45] and optical spectroscopy [38,46,47] provided the necessary evidence that CO is accompanied by lattice effects, attributed to a collective shift of the anions [17].

Pouget proposed [17] two different directions for the anion shift. First, the anion moves along the c -direction towards the methyl groups, as indicated by black arrows in Figure 3a,b. The resulting deformation of the methyl end-groups polarizes the hydrogen-bond network leading to a displacement of charge in the σ -bonds connected to the H-bonds. This indirectly stabilizes the excess of π -holes on the corresponding TMTTF molecule as indicated by a red ellipsoid, whereas blue ellipsoids mark charge-poor molecules (Figure 3).

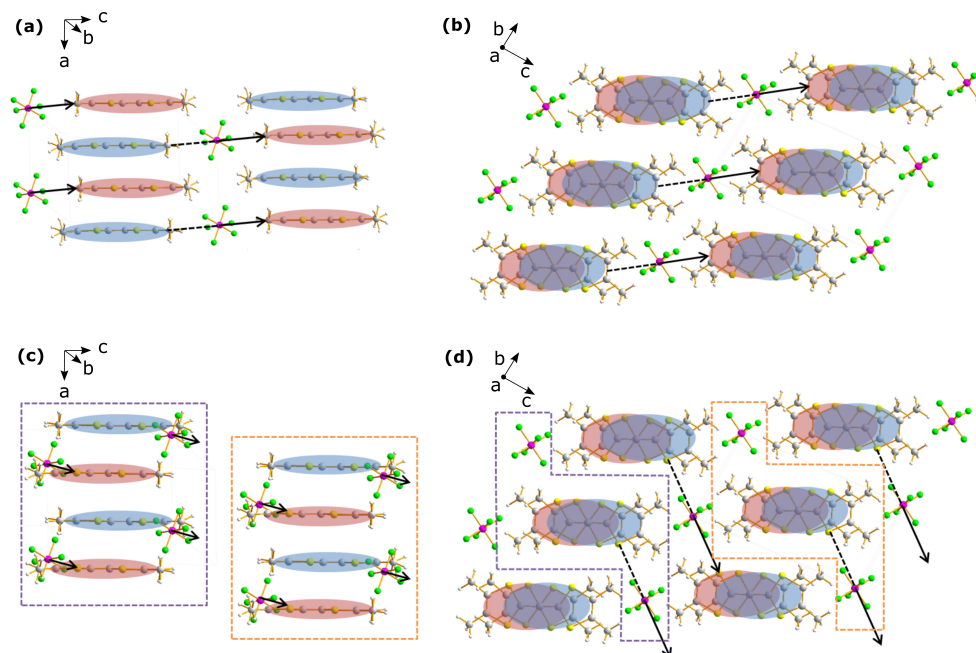


Figure 3. The anions shift along the $b + c$ direction towards the methyl groups and towards the sulfur atoms, as suggested by Pouget [17]. Charge-rich TMTTF molecules are indicated by a red ellipsoids whereas blue ellipsoids mark charge-poor molecules. (a) View in the ac -plane and (b) along the a -axis onto the cb -plane. The shift of the anions towards the S-atoms of the nearest TMTTF molecule depicted (c) in the ac -plane and (d) in the cb -plane. The polygons formed by the purple and orange dashed lines in panel d indicate which anion stacks are shown in the previous frame c.

Several observations support this suggestion of an anion shift with a strong contribution along the *c*-direction. First of all, thermal expansion measurements exhibit a clear anomaly at T_{CO} , which is most pronounced along the *c*-axis [43]. Secondly, the coupling between the methyl groups and the anions is mostly in the *bc*-plane. Furthermore, deuteration of the methyl groups significantly increases T_{CO} . The heavier mass slows the lattice dynamics and weakens the coupling between the anions and terminating endgroups (Figure 4); thus CO can be stabilized already at higher temperatures [23].

The second proposed translation of the anions [17] is towards the closest sulfur atom of a TMTTF molecule, indicated by black arrows in Figure 3c,d. This goes hand in hand with the enhanced π -hole density at the corresponding TMTTF molecule. NEXAFS measurements clearly show the strengthening of the S-F bonds [48].

Both shifts are supposed to increase the charge concentration on the corresponding TMTTF molecule. It is energetically favorable that the second neighboring TMTTF molecule contains less positive charge. Hence, by minimizing the electrostatic energy between the anion stacks and adjacent TMTTF stacks, a three-dimensional charge pattern is established that is crucial for stabilizing CO [23,43]. In fact, temperature-dependent transport measurements [4] clearly show the opening of a CO gap along all three crystallographic directions providing evidence for this three-dimensional charge pattern due to inter-stack coupling mediated by the anions.

Some further considerations have been published, which should be mentioned here. First, the anion shift accompanying CO does not introduce the tetramerization [23]. Second, although the anions do shift at the CO transitions, they are still considered to exhibit a random rotational motion depending on the temperature [17].

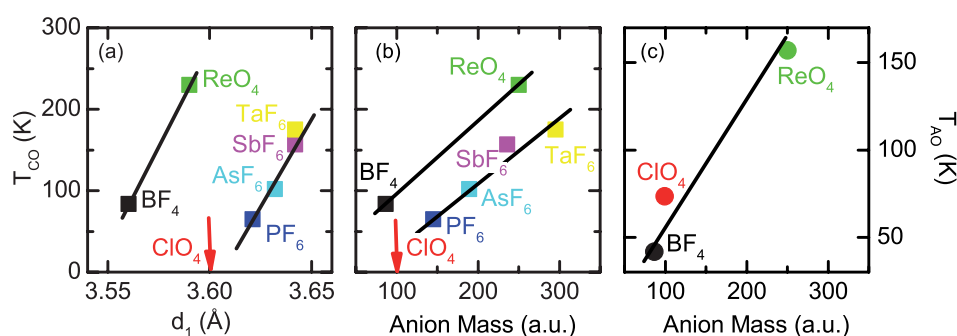


Figure 4. Dependence of the charge order temperature T_{CO} (colored squares) and anion order temperature T_{AO} (colored circles) for various Fabre salts $(TMTTF)_2X$ with different X as indicated. (a) T_{CO} plotted versus the distance between the TMTTF molecules d_1 along stacking direction determined at room temperature. Here, octahedral and tetrahedral salts fall on two different lines. Although the octahedral anions exhibit larger values for d_1 , T_{CO} is lower compared to the tetrahedral salts. The octahedral anions are larger (Table 1) resulting in an increased value of d_1 . The anion-TMTTF stack coupling increases due to the larger anions, and the match between anion and cavity symmetry; thus thermal fluctuations prevail upon the electronic correlations giving rise to CO down to lower temperatures. (b) Plot of T_{CO} versus the mass of the anions. A monotonic increase of T_{CO} with anion mass is observed, which is attributed to less effective motion of heavy anions due to thermal fluctuations and, consequently, a less disordered anion potential influencing electronic correlations within the TMTTF stacks. The octahedral and tetrahedral salts fall on two distinct lines due to different coupling between the anions and the TMTTF stacks. (c) For the anion ordering temperature observed in the tetrahedral $(TMTTF)_2X$ salts, an increase of T_{AO} with the anion mass is observed. At a specific temperature, heavy anions are less affected by thermal fluctuations. Consequently, the anion orientation is locked permanently for heavier anions at higher temperatures. As a result, anion order occurs at higher temperatures for heavy anions.

Having established the anion shift, we now have to pose the question whether charge order can still be understood as a phenomenon inherent to the one-dimensional TMTTF stacks as described by

the extended Hubbard model, or whether a more advanced theoretical treatment is required including the contribution of the lattice in general and the anions in particular. In other words, we have to find out whether the Coulomb attraction between the negative charge located on the anion-ligand with shortest S-F contact is crucial for charge order, or whether it only stabilizes the arrangement. It has been proposed, that the shortest anion-ligand to sulfur distance $d_{\text{AL-S}}$ is the parameter determining CO [4,18], in contrast to a purely electronic picture, which implies that the distances between the TMTTF molecules, d_1 and d_2 , are decisive. Recent spectroscopic and structural investigations could shed light on this issue [18,23]. In the following we give a short overview on the different approaches and on the studies focusing on the structural aspects of the CO transition.

Table 1. Overview on the transition temperatures T_{CO} and T_{AO} , as well as on the room-temperature structural data of various $(\text{TMTTF})_2X$ salts with octahedral and tetrahedral anions X . Here $d_{\text{AL-S}}$ is the shortest distance between the anion-ligand (F or O) and the sulfur atom. d_1 and d_2 denote the distances between planes defined by the TMTTF molecules within one stack [9,11–13,18]. Hence, $(d_1 - d_2)/(d_1 + d_2)$ denotes the structural dimerization along the stacks determined by the distance between the TMTTF molecular planes; it does not take into account any displacement of the molecules along the b or c direction. In contrast to that, δ_{struc} and δ_{elec} are determined by ab-initio DFT calculations based on X-ray structural data [49,50]. δ_{struc} corresponds to a structural dimerization as well, which is defined by the distance between the centers of mass in each TMTTF molecule. $\delta_{\text{elec}} = 2|t_1 - t_2|/(t_1 + t_2)$ explicitly takes into account the overlap of the transfer integrals t_1 and t_2 . The unit cell volume is listed as V_{unitcell} [9,11–13]. The parameter R_0 denotes the thermochemical radius of the monovalent anion [51]; although calculated for a salt with 1:1 stoichiometry, we consider this as a valid estimate for the anion size. The anion volume is listed as V_{anions} following [52]. In the last row the anion mass m_A is given in atomic units.

Anion X	PF_6	AsF_6	SbF_6	TaF_6	BF_4	ClO_4	ReO_4
T_{CO} (K)	67	102	157	175	84	-	230
T_{AO} (K)	-	-	-	-	41.5	73.4	157
$d_{\text{AL-S}}$ (Å)	3.30	3.27	3.21	3.215	3.28	3.45	3.05
d_1 (Å)	3.621	3.632	3.642	3.642	3.56	3.60	3.59
d_2 (Å)	3.527	3.524	3.526	3.534	3.54	3.51	3.57
$\frac{d_1 - d_2}{d_1 + d_2}$ (10^{-2})	1.32	1.51	1.62	1.51	0.28	1.27	0.28
δ_{struc}	0.040	0.041	0.041	-	0.028	0.04	-
δ_{elec}	0.230	0.110	0.298	-	0.336	0.616	-
V_{unitcell} (Å ³)	676.6	697.7	702.9	706.52	648.5	654.8	679.5
R_0 (pm)	242	243	252	250	205	225	227
V_{anions} (Å ³)	70.6	-	81.8	-	51.6	54.7	64.8
m_A (au)	144.96	188.91	235.75	294.94	86.80	99.45	250.21

In Table 1 we summarize electronic and structural parameters determined from literature data. For the octahedral anions, T_{CO} rises with anion size (and mass) $d(\text{PF}_6) < d(\text{AsF}_6) < d(\text{SbF}_6) < d(\text{TaF}_6)$; the same is found for the salts with tetrahedral anions. Moreover, a larger anion diameter correlates with a shorter sulfur-anion-ligand distance $d_{\text{AL-S}}$ and larger intra-stack distances between the TMTTF molecules d_1 and d_2 . Regarding the structural dimerization $\frac{d_1 - d_2}{d_1 + d_2}$ and T_{CO} , no clear trend can be seen [18,49,50]. So far, T_{CO} scales with both, $d_{\text{AL-S}}$ and d_1 , impeding a simple answer of the question posed above.

In Figure 5a the charge disproportionation 2δ is plotted as a function of the CO temperature T_{CO} . Interestingly, both the salts with tetrahedral and with octahedral anions fall onto the very same line, providing strong indications that CO is independent on anion symmetry and emerges from the electronic interaction and one-dimensional physics inherent to the TMTTF stacks [23]. This conclusion complies with the extended Hubbard model and theories based on it; where structural peculiarities are

disregarded [6]. Along these lines the competition between the nearest-neighbor Coulomb repulsion V and the bandwidth $W = 4t$ is crucial for CO, wherein the transfer integral t sensitively depends on the distance between TMTTF molecules.

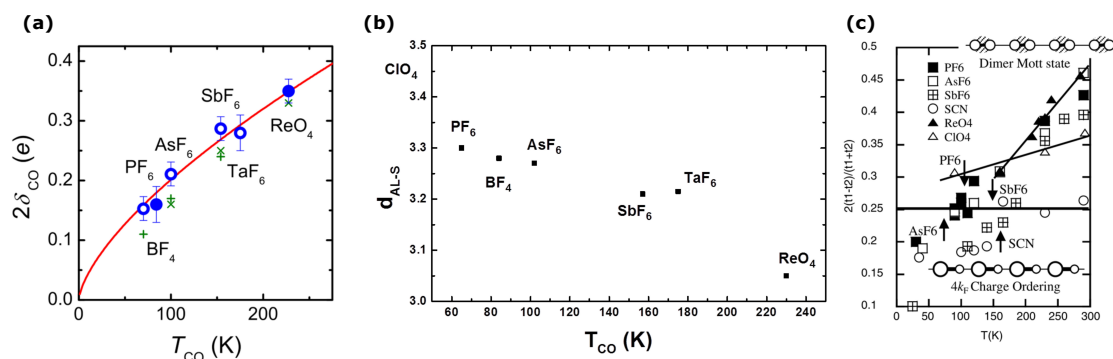


Figure 5. (a) Charge disproportionation 2δ of the $(TMTTF)_2X$ salts with different anions X plotted versus the CO transition temperature T_{CO} . The open circles [38,53] and closed circles [23] were determined by optical spectroscopy on the octahedral anions PF_6 , AsF_6 , SbF_6 , TaF_6 , and tetrahedral anions BF_4 and ReO_4 , respectively; the green crosses and green plus signs were measured by NMR [37,54,55] and Raman spectroscopy [38,56], respectively. The red line corresponds to $2\delta \propto T_{CO}^{2/3}$. Most important, all salts fall onto this line independent on the anion symmetry. (b) The shortest distance d_{AL-S} between the sulfur atom of the organic molecule and the anion-ligand is evaluated at room temperature and plotted in dependence on the charge-order transition temperature T_{CO} . All salts exhibiting CO fall on a line, indicating a linear decrease of T_{CO} as the spacing d_{AL-S} increases. (c) Temperature dependence of the bond dimerization $\frac{2|t_1-t_2|}{(t_1+t_2)}$ taken from Reference [15], wherein the transfer integrals t_2 and t_1 were obtained by applying the extended Hückel model on temperature dependent X-ray data.

To countercheck, in Figure 5b the distance d_{AL-S} is plotted versus T_{CO} . For all salts we find a linear relation of falling transition temperature and increasing distance, independent on the symmetry of the anions. Note, the values given in Table 1 and plotted in Figure 5b are determined at ambient conditions; they change upon cooling and the application of pressure.

Figure 5c presents the temperature dependence of the electronic bond dimerization $\delta_{elec} = \frac{2|t_1-t_2|}{(t_1+t_2)}$, which is proportional to the electronic dimerization δ_{elec} , considering that the transfer integrals t_2 and t_1 are calculated by the extended Hückel model on temperature dependent X-ray data [15]. Most importantly, the dimerization decreases with lowering the temperature, fully consistent with the findings of Reference [50]. It is concluded that CO sets in below a critical bond dimerization of 0.25. This picture explains the absence of CO in $(TMTTF)_2ClO_4$, however, $(TMTTF)_2BF_4$ is not included. There also remains a discrepancy between the observed value of about 0.37 for $(TMTTF)_2ReO_4$ with $T_{CO} = 230$ K.

In a more advanced approach, the influence of structural effects on charge ordering in the $(TMTTF)_2X$ salts was investigated by ab-initio DFT calculations based on pressure- and temperature-dependent X-ray data [49,50]. No systematic relation was observed as far as T_{CO} and the structural dimerization is concerned, i.e., the distance between the TMTTF molecules. For the electronic dimerization δ_{elec} , however, they find an increased value for $(TMTTF)_2ClO_4$ compared to the other salts, that explains the absence of CO in this particular salt. Besides the distance of the molecular planes, δ_{elec} also takes into account the differences in the orientation and size of the transfer integrals. When the electronic dimerization increases, CO is suppressed and can even be absent as in the case of $(TMTTF)_2ClO_4$.

We can conclude this short overview by emphasizing the importance of ab-initio DFT calculations based on detailed temperature-dependent X-ray data for all (TMTTF)₂X salts. This way we can unambiguously determine which role lattice effects play in general and the anions in particular on the charge-order transition.

2.3. Anion Order

In addition to charge order, the (TMTTF)₂X salts with non-centrosymmetric anions X = SCN, SFO₃, NO₃, BF₄, ClO₄, and ReO₄ undergo an ordering of the anions at T_{AO}; here we focus on the tetrahedral counter ions. At room temperature, the octahedral and tetrahedral anions exhibit random translational and rotational movement caused by thermal fluctuations [22]. As the temperature is lowered, the tetrahedra do not fit into the cavities formed by the methyl end-groups due to their non-matching symmetry resulting in a stochastic anion orientation [17]. This orientational disorder is resolved at T_{AO} by AO, a structural phase transition orienting the anions within the cavities.

For the (TMTTF)₂X salts with X = BF₄, ClO₄ and ReO₄, the ordering of the anions is a first-order transition breaking the room temperature symmetry and doubling the lattice periodicity [4,18]. The resulting superstructure exhibits a reduced wave vector of $q_{AO} = (\frac{1}{2}, \frac{1}{2}, \frac{1}{2})$ [16,17,57]. AO is detected by several methods: in resistivity measurements a kink-like feature is observed with a corresponding hysteresis [4], a pronounced peak or shoulder is seen in dielectric spectroscopy [32,36,58], and the optical spectra are distinctly modified [23]. In the case of (TMTTF)₂ClO₄ charge disproportionation 2δ occurs right at the anion order [23]. As can be seen from Table 1, T_{AO} rises with increasing anion volume and mass.

It is instructive to look at the sibling compound (TMTSF)₂X, where the AO takes place at T_{AO} = 24 K for X = ClO₄ and 180 K for ReO₄ [57,59–61]. In general the selenium analogues possess a larger bandwidth, compared to the (TMTTF)₂X salts and therefore the anion potential has only smaller influence. While the former compound orders in a $q_{AO} = (0, \frac{1}{2}, 0)$ fashion, the latter one also exhibits a first-order phase transition with a wave vector $q_{AO} = (\frac{1}{2}, \frac{1}{2}, \frac{1}{2})$; interestingly a high-pressure phase with $(0, \frac{1}{2}, \frac{1}{2})$ coexists for $p > 10$ kbar [62]. For both compounds, the solid solution of TMTTF and TMTSF reveals several instabilities, broadens and shifts the AO transition [61,63–65]. A large number of studies have been devoted to the occurrence of superconductivity in (TMTSF)₂ClO₄ as the cooling rate is varied in order to retain anion disorder to low temperatures [66–69]. To the best of our knowledge, similar studies have not been performed on the Fabre salts.

Figure 6 illustrates our present understanding of the structural modifications taking place at the AO transition [17,18,23]. Due to their non-centrosymmetric shape, the tetrahedral anions exhibit only a single anion-ligand to sulfur link along the $(-b + c)$ -direction, indicated by the black dashed line. This defines the direction along which the tetrahedra preferably reorient: one corner points along the anion-ligand to sulfur link towards the nearest S atom of the closest neighboring TMTTF molecule. Simultaneously, the other three anion ligands lie in a plane matching the symmetry of the methyl cavity.

A great many experiments provided compelling evidence that the anions are not statistically oriented along one of the two possible directions towards the nearest S atoms but exhibit long-ranged order, resulting in a 0110 charge pattern and tetramerization of the TMTTF stacks as sketched in Figure 6. Structural refinements on (TMTTF)₂ReO₄ revealed the staggered orientation of the anions along the [111]-direction and the tetramerization with intra-stack distances $d_1 \approx 3.45$ Å, $d'_2 \approx 3.6$ Å and $d''_2 \approx 3.48$ Å [70]. The molecular tetramerization was also observed by angular-dependent X-ray near-edge structure (XANES) measurements [27]; in addition, they reveal a slight shift and deformation of the ReO₄ anions. For all salts with tetrahedral anions X = BF₄, ClO₄ and ReO₄, electron spin resonance (ESR) spectroscopy sees a drop of the spin susceptibility right at T_{AO} that is attributed to the formation of a singlet-triplet gap upon tetramerization [71–73]. Most recently, infrared spectroscopy could confirm the 0110 charge pattern by looking at the molecular vibrations [23]; more comprehensive investigations on this issue are under way [74].

Albeit a precise and complete microscopic picture of the AO transition could not be reached yet, there is wide agreement that Coulomb interactions between the anions and the TMTTF stacks are the driving force [17]. The orientation and slight deformation of the anions gives rise to a periodic electrostatic potential influencing the charge distribution on the TMTTF molecules. This anion potential is most pronounced along the sulfur to anion-ligand link and thus the staggered orientation of the anions imposes the 0110 charge pattern onto the TMTTF stacks. As seen from Table 1, there is no monotonic dependence of T_{AO} on d_{AL-S} ; we should mention, however, that d_{AL-S} is determined at room temperature and one should consider the distance right at the respective AO transition. It is not fully clear to what extent the 0110 charge pattern actually minimizes the Coulomb repulsion within the TMTTF stacks. The contribution of the anion potential cannot be determined precisely without detailed structural data in dependence on temperature covering the AO transition. Finally we would like to draw the attention on the effect of isotope substitution, since T_{AO} seems not to change appreciably upon deuteration [36].

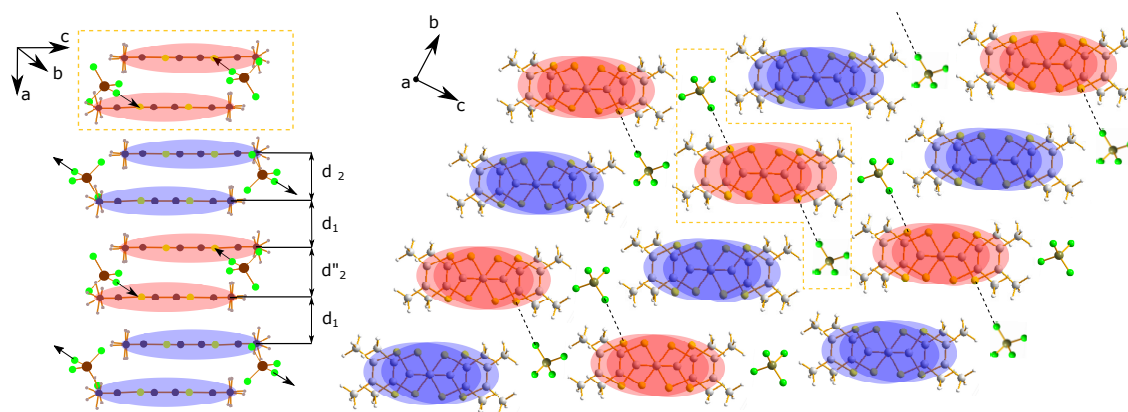


Figure 6. Scheme of the anion arrangement for the tetrahedral $(TMTTF)_2X$ salts as $T < T_{AO}$. Upon AO, the anions re-orient in the methyl cavities along the anion-ligand sulfur link in $(-b + c)$ -direction, represented by the black dashed line, forming long-range order. Coulomb attraction between the anion-ligand and the charge on the TMTTF molecule results in a 0110 charge pattern; the red and blue ellipsoids mark charge-rich and charge-poor TMTTF molecules, respectively. The polygon formed by the dashed orange line indicates which anion stacks are shown on the left side, illustrating the charge pattern along the stacking direction. In addition to a reorientation of the anions, a shift along the anion-ligand sulfur link occurs as well; this is not included here.

2.4. Deuteration

The replacement of hydrogen by deuterium in the methyl end-groups of the TMTTF molecule has only minor influence on the anion order but increases T_{CO} [75–77]; hence deuterated $(TMTTF)_2X$ salts provide valuable information on the ordering mechanisms. It was pointed out recently [23] that with increasing anion size or mass, the effect of deuteration on the CO transition diminishes. Defining the temperature shift $\Delta T_{CO} = T_{CO,D} - T_{CO}$, where $T_{CO,D}$ and T_{CO} are the transition temperatures for the deuterated and hydrogenated crystals, respectively, the change in transition temperature is strongest for small anions, as illustrated in Figure 7a. This important relation provides compelling evidence that charge order – considered as a purely electrostatic effect – is crucially affected by dynamic anion fluctuations. A simple relation is found for all TMTTF salts studied: $T_{CO,D}^2 = T_{CO}^2 + D^2$.

It is important to note the structural aspect that dimerization decreases upon deuteration. Starting with equally spaced TMTTF molecules in an isolated stack, dimerization is imposed by

the anions. The coupling of the thermally fluctuating anions to the TMTTF stacks takes place via the terminal methyl groups, i.e., it is mediated by hydrogen bonds. At elevated temperatures, the methyl groups and the anions both require more space due to thermal fluctuations; their stronger interaction enhances the anion-TMTTF coupling. By deuterium substitution the methyl-group motion is slowed down, reducing the coupling to the counterions. As a consequence, the dimerization is smaller for d_{12} -TMTTF salts compared to the hydrogenated analogues. This also explains the concomitant enhancement of T_{CO} .

Anion order takes place at lower temperatures when the anions and the methyl groups fluctuate less and their dynamic interaction is of minor relevance. Instead, it is more important to consider the static Coulomb interaction between the monovalent anions and the charge spread on the TMTTF molecules, mainly located at the S atom and the C=C double bonds. Since the electrostatic interaction is not affected by deuteration, the influence of the anions does not change due to this isotope substitution.

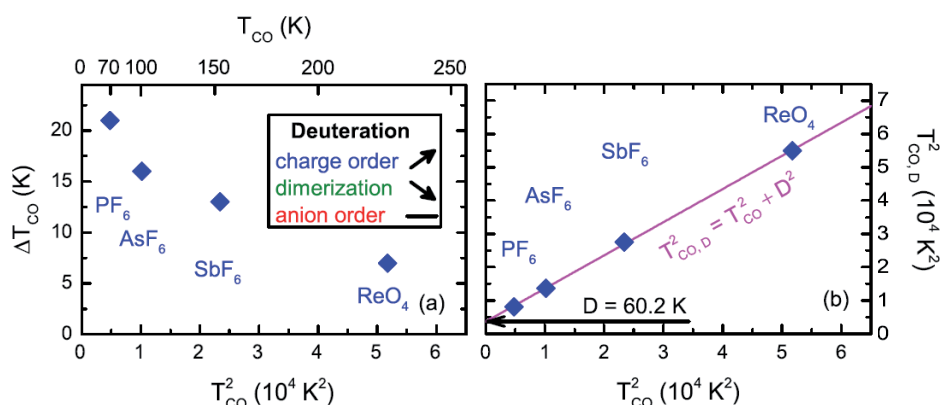


Figure 7. Effect of deuteration on charge order observed in $(TMTTF)_2X$. (a) For several anions $X = PF_6$, AsF_6 , Sb_6 and ReO_4 , the change in the transition temperature $\Delta T_{CO} = T_{CO,D} - T_{CO}$ is plotted versus the square of the CO transition temperature T_{CO}^2 of pristine crystals. The increase is most pronounced for small and light anions. The inset indicates that deuteration rises the CO temperature, deminishes dimerization, but has no effect on AO. (b) Plotting $T_{CO,D}$ over T_{CO} clearly reveals the dependence $T_{CO,D}^2 = T_{CO}^2 + D^2$ with $D = 60.2 K$. The data are taken from Reference [75,77]; the plot follows Reference [23].

3. Experimental Details

Single crystals of $TMTTF_2X$ salts with $X = BF_4$, ClO_4 and ReO_4 were grown by the standard electrochemical methods using an H-type glass cell at ambient temperature and inert atmosphere. Platinum plates with an area of approximately $3 cm^2$ served as electrodes and a sand barrier was introduced to reduce diffusion. By applying a constant voltage of 1.5 V, a current between 9.2 and 13.4 μA was drawn through the solution. The growth of the needle-shaped single crystals of typical dimensions $(2 \times 0.5 \times 0.1) mm^3$ took several months. Since the crystal shape does not correspond to the triclinic symmetry of the crystal structure, b' denotes the projection of the b -axis perpendicular to the a axis, and c^* is chosen orthogonal to the ab -plane.

In order to perform the electrical transport measurements, small gold contacts were evaporated onto the natural crystal surface and thin gold wires were attached to them by carbon paste. The dc experiments applied the four-point method. Pressure-dependent measurements were carried out by means of a clamp-type pressure cell using Daphne 7373 oil as pressure medium. Daphne 7373 is the favored pressure medium for this kind of experiments because it conveys hydrostatic pressure and $(TMTTF)_2X$ crystals are inert to it. For all applied pressures the pressure medium stays fluid at room temperature, relevant shearing forces seem to appear only when cooling through the freezing temperature at pressures between 0–3 kbar. Temperature-dependent transport measurements were carried out in a standard helium bath cryostat. The inherent pressure loss upon cooling was recorded

continuously in-situ by an InSb semiconductor pressure gauge, as illustrated in Figure 8. The dielectric measurements were performed with two contacts in a pseudo four-point configuration by means of an Agilent 4284 Impedance Analyzer (20 Hz–1 MHz). For both measurement techniques, the applied voltage was in the mV range to avoid heating and ensure measurements in the Ohmic regime.

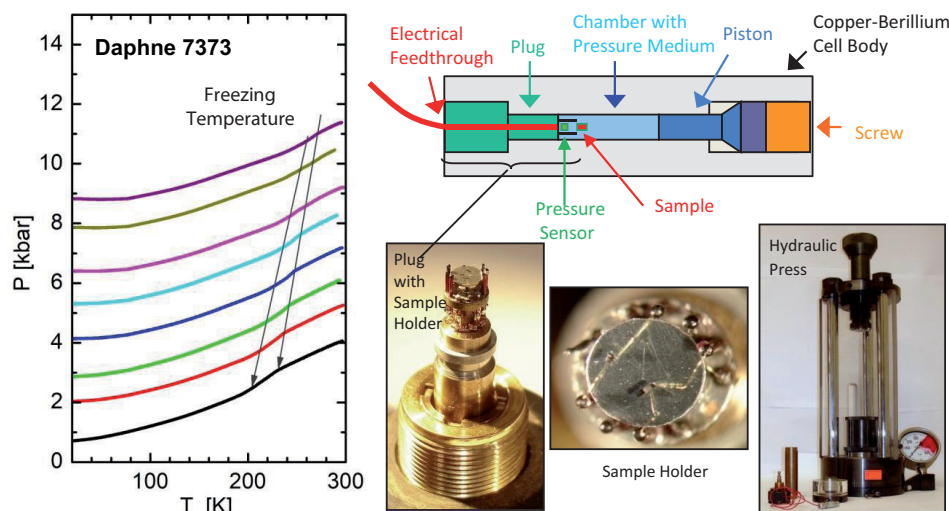


Figure 8. Left panel: Pressure loss of Daphne 7373 oil during cooling; the arrows mark the temperature range of freezing. The data were recorded in a Copper-Beryllium cell by four-point resistance measurement of an InSb pressure sensor. Right panel: Sketch of the actual pressure cell used and photos of the sample holder, and the hydraulic press.

4. Electrical Transport under Pressure

The physical properties of the $(\text{TMTTF})_2\text{X}$ family have been widely studied for several decades [78–81], however most of the work dealt with centrosymmetric anions. Here we advocate that the structural phase transition should not be considered an additional complication but an opportunity to gain more insight on the effect of the lattice on the electronic properties; there is no question, however, that further investigations are needed. In the following we will present the first complete set of systematic dc measurements under hydrostatic pressure of the three most common $(\text{TMTTF})_2\text{X}$ with tetrahedral anions ($\text{X} = \text{BF}_4, \text{ClO}_4, \text{ReO}_4$). After detailed discussions of $\rho(T, p)$ for each particular compound, we will compare the rather diverse characteristics.

4.1. $(\text{TMTTF})_2\text{ClO}_4$

From Table 1 we see that $\text{X} = \text{ClO}_4$ is placed between $\text{X} = \text{BF}_4$ and ReO_4 with respect to the anion size. From the charge transfer salts with octahedral anions we know that T_{CO} increases with anion radius [4,18]. The same is expected for the tetrahedral anions. $(\text{TMTTF})_2\text{ClO}_4$ is in so far particular, as it does not exhibit the charge order typical for all other Fabre salts. As far as the anion transition is concerned, it follows strictly the expected relation for the tetrahedral anions: $T_{\text{AO}}(\text{BF}_4) < T_{\text{AO}}(\text{ClO}_4) < T_{\text{AO}}(\text{ReO}_4)$.

The pressure dependence of $\rho(T)$ is affected by the absence of CO showing extraordinary features. In Figure 9 the electrical resistivity $\rho_a(T, p)$ and $\rho_c(T, p)$ are displayed for pressures up to 11.6 kbar in panels a,b and d respectively. At ambient pressure, $\rho_a(T)$ develops the well-known activated temperature dependence for $T < T_\rho \approx 260$ K (localization temperature) and shows a distinct jump to lower values at $T_{\text{AO}} \approx 73$ K [4]. It is interesting to note a change in slope of $\rho_a(T)$ that appears around 40 K. Applying hydrostatic pressure, the local minimum at T_ρ disappears as well as the jump at T_{AO} . Whereas the former may be assessed as an artifact caused by the temperature-dependent pressure loss due to the pressure media in the cell (Daphne oil 7373, see Figure 8), the latter is inherent

to $(\text{TMTTF})_2\text{ClO}_4$. For increasing pressure, the AO transition smears, broadens and moves to lower temperatures, developing a distinct valley of low resistivity. Concurrently the onset of the transition $T_{\text{AO-max}}$ follows the trend of T_{AO} , accompanied by the development of steep increase of $\rho(T, p)$ at T_{M} , which is related to the lower bound of the minimum.

At $p \approx 10$ kbar the trend stops; $T_{\text{AO-max}}$ and T_{M} do not significantly shift in temperature any more when p increases further. The mechanism triggering the valley seems to come to a halt. As can be seen in Figure 9b, the valley is gradually filled. At the maximum pressure applied, $p = 11.6$ kbar, the minimum has somehow disappeared completely. Instead for high pressures a second peak develops at about 40 K, which does not shift in temperature for $p > 11$ kbar; this feature progressively dominates the temperature dependence of $\rho(T)$. This behavior is observed in both directions, for $\rho_a(T, p)$ and $\rho_c(T, p)$, as seen by comparison of panels b and d. In Figure 10 we take a closer look at the pressure range from 10.0 to 11.6 kbar. The appearance of the second peak is accompanied by a hysteretic behavior in the temperature-dependent resistivity on both sides of the valley. Multiple temperature cycles reveal fluctuations in $\rho_a(T)$ not observed in other cases.

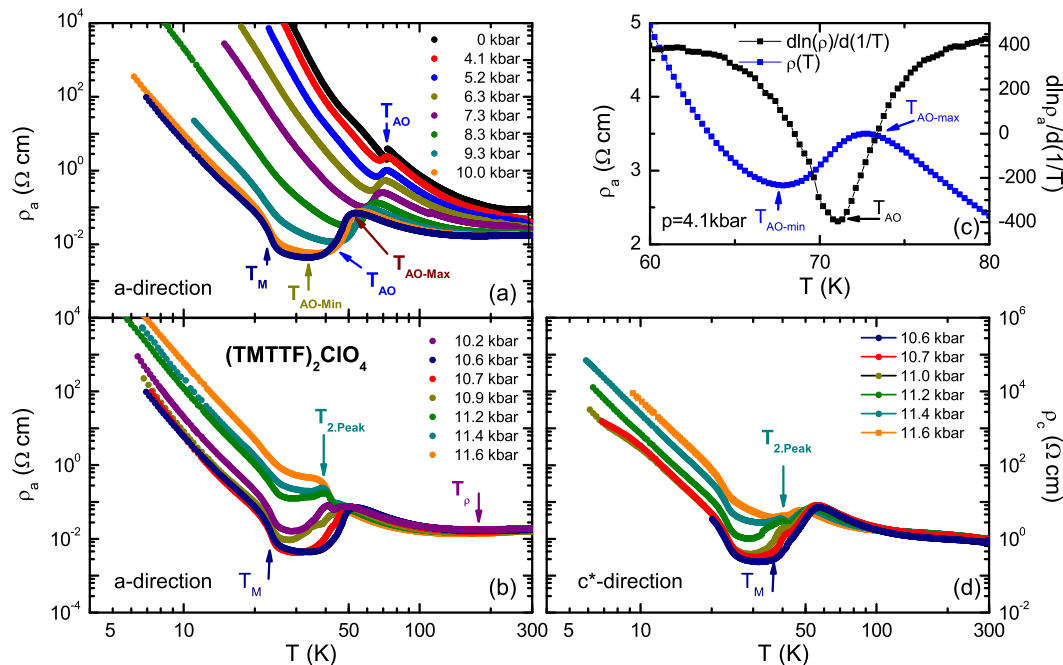


Figure 9. Pressure evolution of the temperature-dependent electronic transport of $(\text{TMTTF})_2\text{ClO}_4$. (a) dc resistivity as a function of temperature for ambient conditions and for hydrostatic pressures up to 10.0 kbar measured along the stacking direction a . (b) For higher pressure values a more complex behavior of $\rho_a(T, p)$ is observed. (c) For the example taken at $p = 4.1$ kbar, we illustrate how the different parameters of the anion ordering transition were extracted from $\rho(T, p)$ and its derivative with respect to inverse temperature $1/T$. (d) Temperature dependence of the perpendicular resistivity $\rho_c(T, p)$ for the high-pressure range.

In the phase diagram displayed in Figure 11a, we summarize the different phases, transitions, and appearing features as extracted from our $\rho(T, p)$ data. At elevated temperatures $(\text{TMTTF})_2\text{ClO}_4$ behaves like a low-dimensional metal with $d\rho_a/dT > 0$ along the stacking direction and $d\rho_c/dT < 0$ perpendicular to the stacks. Between 250 and 150 K charge localization takes place at T_{ρ} . While the metal-like behavior in $\rho_a(T, p)$ for $T > T_{\rho}$ is obvious at $p = 0$, it gets masked for finite but intermediate pressures; interestingly, the localization temperature is recovered at high p values. According to Figure 8 the temperature-dependent pressure loss is reduced as the applied pressure increases; hence this effect influences $\rho(T)$ less. For the $p = 9.3$ kbar curve, we can clearly identify a range of metallic

behavior by $d\rho_a(T, p)/dT > 0$. For increasing pressures, the minimum in $\rho(T)$ at T_p is reduced. T_p extracted in this manner specifies the upper limit of the inherent localization temperature of $(\text{TMTTF})_2\text{ClO}_4$. Since in the perpendicular direction $d\rho_c(T, p)/dT < 0$ for the whole investigated pressure and temperature range, our data identify the high-temperature phase of $(\text{TMTTF})_2\text{ClO}_4$ as a low-dimensional metal. The subsequent phase is an insulating one; nothing hints towards any inherent changes in the material down to the anion ordering. No indications towards charge order are detected.

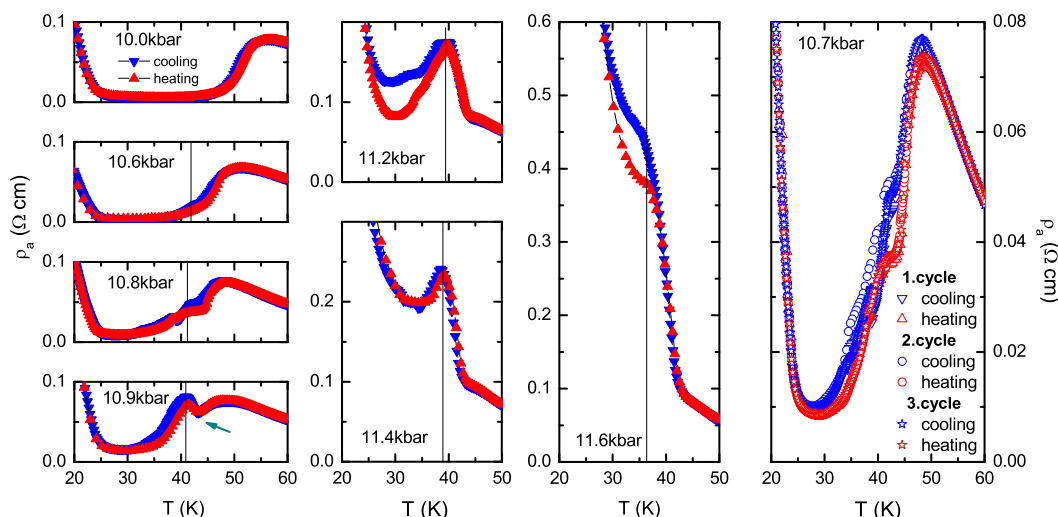


Figure 10. Magnification of the high-pressure resistivity along the a -axis of $(\text{TMTTF})_2\text{ClO}_4$ in the temperature range of T_{AO} . For pressure between 10.2 – 11.7 kbar, a second peak in $\rho_a(T)$ appears. Simultaneously at the anion ordering $\rho_a(T)$ exhibits a distinct hysteresis and fluctuations.

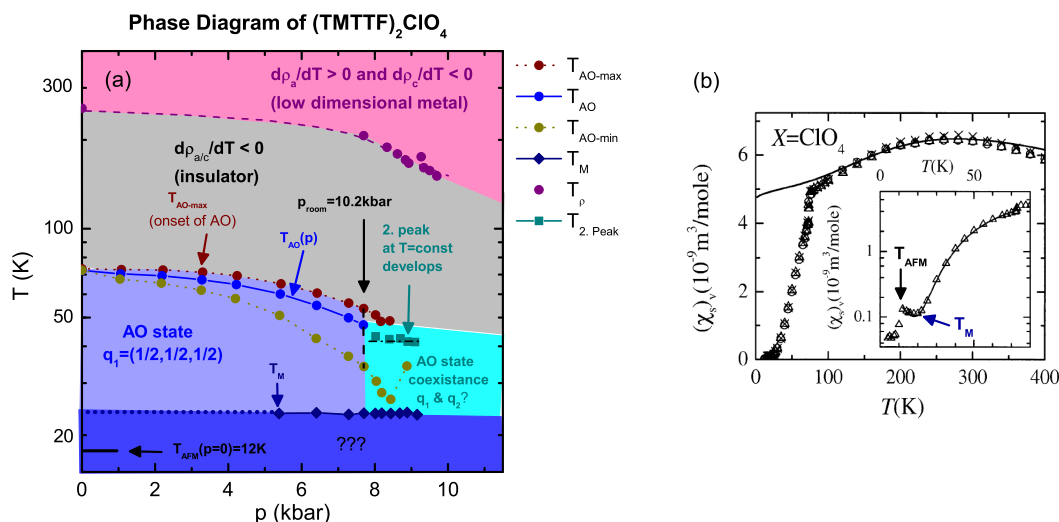


Figure 11. (a) The phase diagram of $(\text{TMTTF})_2\text{ClO}_4$ as obtained from resistivity measurements indicates various phase transitions. (b) Temperature-dependent susceptibility of $(\text{TMTTF})_2\text{ClO}_4$ as obtained from electron spin resonance (ESR) measurements (taken from Dumm et al. [82]). Two distinct drops in the ESR intensity can be identified, one at the AO transition and the other at the antiferromagnetic order $T_{\text{AFM}} = 12$ K. The onset of the plateau appears around $T \approx 20$ K (indicated by the blue arrow), which coincides with the steep increase of the resistivity at T_{M} .

The onset of the AO transition, $T_{\text{AO-max}}$, is defined by the local maximum in $\rho(T)$ followed by a sharp drop; the AO temperature T_{AO} is given by the steepest decline of $\rho(T)$ between $T_{\text{AO-max}}$ and the local minimum at $T_{\text{AO-min}}$. This is illustrated in Figure 9c in full detail, where also the derivative

$d \ln\{\rho_a\}/d\left(\frac{1}{T}\right)$ is plotted in the Arrhenius-like manner. The AO transition becomes obscured, when the second peak starts to grow. This additional feature is first visible as pressure exceeds 10 kbar. It always seems to be located at $T \approx 40$ K, with no significant shift for varying pressure. It is interesting to compare the structural properties with the sister compound $(\text{TMTSF})_2\text{ClO}_4$, which can be turned from a $T_c = 1$ K superconductor to an antiferromagnetic SDW insulator by suppression of the $q_2 = (0, \frac{1}{2}, 0)$ anion order at $T_{\text{AO}} = 24$ K by rapid cooling [61]. The pronounced hysteresis and fluctuations might point towards the development of an AO with another superstructure at $T = 40$ K. Recalling the observation of different superstructures with pressure and disorder in $(\text{TMTSF})_2\text{ReO}_4$ [62], we could imagine a coexistence of the conventional AO superstructure $q_1 = (\frac{1}{2}, \frac{1}{2}, \frac{1}{2})$ and a new, but weaker one with a different q vector also for $(\text{TMTTF})_2\text{ClO}_4$ [13].

It might be worth to have a closer look on the temperature T_M defined by the lower bound of the resistivity valley, since this transition does not shift in temperature for the entire pressure range. The strong increase in $\rho(T)$ at T_M cannot be related to the transition into the antiferromagnetic state, since for $p = 0$ the corresponding transition occurs at $T_{\text{AFM}} = 12$ K [83] and no feature is visible in the resistivity data at that temperature. It is interesting to note, however, that the increase of $\rho(T)$ at $T = T_M$ coincides with the weak upturn of the magnetic susceptibility after the local minimum in the ESR data (reproduced in Figure 11b) [82]. Although T_M develops only for relatively high pressures, the ESR data are recorded at ambient pressure. Maybe this feature is present even at ambient conditions but masked by the high resistivity due to the strong anion order. We call for further investigations of these relations.

4.2. $(\text{TMTTF})_2\text{BF}_4$

In Figure 12 we present our dc resistivity results $\rho_a(T, p)$ and $\rho_c(T, p)$ for $(\text{TMTTF})_2\text{BF}_4$, the compound with the smallest tetrahedral anion. At first sight, the resistivity of the two crystal directions seems not to differ much, except of the absolute value. Dominated by an activated temperature dependence, a pronounced kink at the CO transition is present for all investigated hydrostatic pressure values. It is followed by an increase in slope for $T < T_{\text{CO}}$. At the anion ordering both $\rho_a(T)$ and $\rho_c(T)$ exhibit a step-like feature, but then continue with more or less the same derivative. As pressure rises, this step-down is washed out and has eventually disappeared completely. The activation energy is significantly reduced for rising pressure. A closer look reveals distinct differences between the transport in the different crystallographic directions: ρ_a and ρ_c . Most obvious, the temperature-dependent dynamics along the a -axis appears about two orders of magnitude higher for all pressures compared to the transport along the c^* -direction. Pressure has a much more severe effect on the perpendicular transport ρ_c than parallel to the stacks, ρ_a . For low temperatures, the high-pressure resistivity becomes almost isotropic.

The analysis of the charge and anion ordering transitions is explained in Figure 12. In panels c and d the derivatives $d \ln\{\rho_a\}/d\left(\frac{1}{T}\right)$ are plotted as a function of temperature in order to define the actual transition temperatures. Here we can also identify differences in the slopes, since this temperature derivative equals the gap size of an activated behavior. The kink in $\rho(T)$ at T_{CO} appears as a clear peak in the derivative. For increasing pressure the CO peak sharpens, it gets more pronounced and shifts to lower T .

For $T \leq T_{\text{CO}}$ and high pressures, we see a steep upturn in resistivity that occurs for $\rho_a(T, p)$ as well as for $\rho_c(T, p)$. It is followed by a clear change of the resistivity slope at T_{AO} . It is interesting to look at the ratio of the resistivity values at the CO transition and those at the AO transition: $\Delta\rho = \rho(T_{\text{AO}})/\rho(T_{\text{CO}})$. Along the stacks, the change is about five orders of magnitude at all pressures; for the c^* -direction, $\Delta\rho$ shrinks from 10,000 at ambient pressure to only about 100 at the highest investigated pressure of $p = 11.5$ kbar. Hydrostatic pressure has a stronger impact on $\rho_c(T, p)$ than on $\rho_a(T, p)$. This picture is supported by the more pronounced loss in activation energy with pressure at $T \leq T_{\text{AO}}$ for the transverse transport $\rho_c(T, p)$ compared to the longitudinal one $\rho_a(T, p)$.

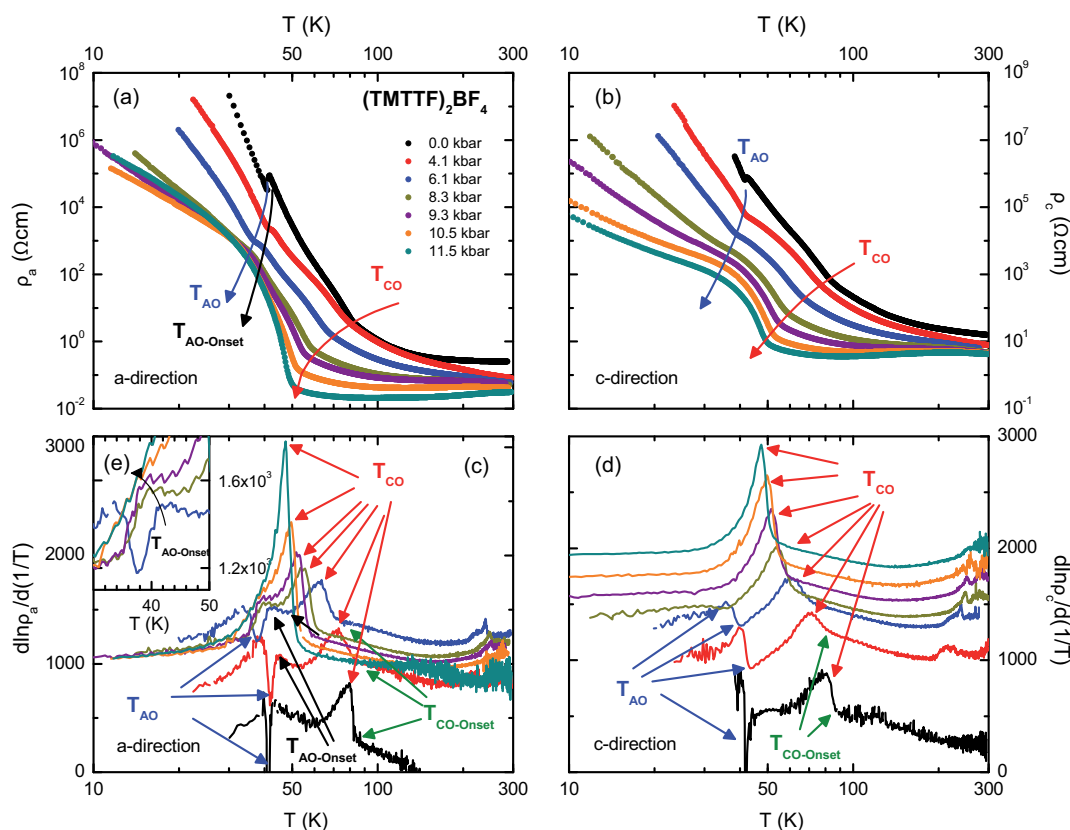


Figure 12. Temperature dependence of the dc resistivity of $(\text{TMTTF})_2\text{BF}_4$ measured for the directions (a) parallel and (b) perpendicular to the stacks when increasing hydrostatic pressure is applied as indicated. Besides the minimum in resistivity at T_ρ , the charge-order transition at T_{CO} and the anion ordering at T_{AO} is clearly observed. The analysis of the data is illustrated in panels (c) and (d) where the temperature derivative $d \ln\{\rho_a\}/d(1/T)$ is plotted for both orientations. The extrema indicate the ordering temperatures T_{AO} and T_{CO} . In addition we define an onset temperature for the charge and anion orders. The inset (e) enlarges the range around the AO temperature.

At T_{AO} , $\rho(T, p)$ undergoes another remarkable change in its behavior that strongly depends on pressure. Under ambient conditions, AO results in a discrete jump in $\rho(T)$ to lower values; since the slope is preserved, the gap size in an activated behavior remains unchanged at the transition. This observation was explained [4] by a reduction of scattering as the anions are locked in the methyl cavities. This jump becomes smooth when pressure is applied; a plateau starts to develop gradually. Increasing pressure further, $\rho(T)$ becomes rather broad for both directions, and eventually the AO transition cannot be identified as a discrete feature any more; what remains is an upturn in resistivity in a wide temperature range. Looking at the derivative in Figure 12c,d, T_{AO} is identified as a sharp peak in the low-pressure range. But for $p \geq 8.3$ kbar this characteristic vanishes. It is interesting to note that the onset of the AO transition at $T_{\text{AO-onset}}$ related to the upturn in $d \ln\{\rho_a\}/d(1/T)$, seen just before T_{AO} (Figure 12c and inset e), can be distinguished up to the highest pressure. For $p = 11.5$ kbar the AO-onset peak is dominated by the strong CO peak coming very close in temperature. Surprisingly, no onset feature of AO is present in ρ_c . Nevertheless, these observations in ρ_a hint that the AO transition might survive even the high hydrostatic pressure. No doubt T_{AO} shifts down in temperature much slower with pressure than T_{CO} .

In Figure 13a,b we focus on the high-temperature regime in order to inspect the metallic behavior and charge localization. For high pressure, $p \geq 10.5$ kbar, both $\rho_a(T)$ as well as for $\rho_c(T)$ exhibit a metal-like temperature dependence. The derivatives plotted in Figure 13c,d evidence a crossing of the zero line at around $T = 100$ K. We should note that in the clamped cell pressure losses might

occur when cooling down from high temperatures, masking the inherent metallic behavior. Thus the second crossing point should be considered with some reservations, when drawing the phase diagram in Figure 13e. We associate the change in slope $d\rho_a(T)/dT$ with the charge localization temperature $T_{loc} \approx 240$ K. With increasing pressure T_{loc} shifts to lower temperatures. For the perpendicular transport, $\rho_c(T)$ exhibits an activated behavior under ambient conditions. The boundary between the metallic regions in Figure 13e therefore indicates a lower limit.

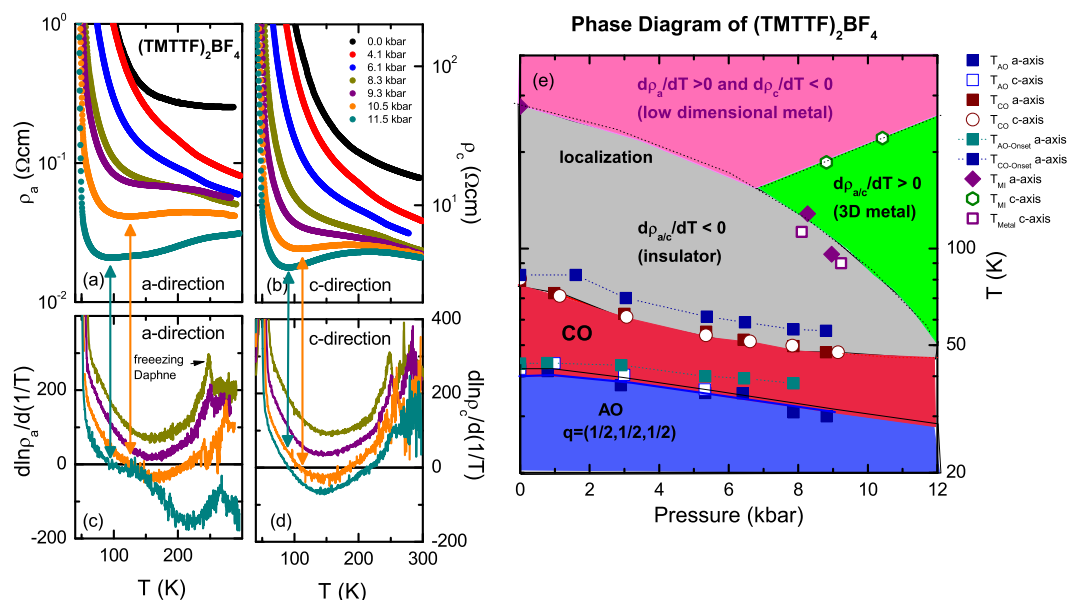


Figure 13. The panels on the left display the temperature dependence of the resistivity of (TMTTF)₂BF₄ measured for different hydrostatic pressure applied with the main focus on the metal-insulator transition and charge localization. (a) The on-chain resistivity $\rho_a(T)$ exhibits the development of a minimum as pressure increases. (b) Resistivity $\rho_c(T)$ perpendicular to the stacks for different pressure values. (c,d) Pressure evolution of the resistivity derivative $d\ln(\rho)/d(1/T)$ as a function of temperature for both orientations. The metal-insulator transition is indicated by the arrows. Also seen is the freezing of the pressure transmitting oil Daphne 7373. (e) In the phase diagram of (TMTTF)₂BF₄ different electronic states are depicted as derived from dc transport experiments. Upon cooling the low-dimensional metal exhibits a charge localization that moves from about room temperature down to below 100 K as pressure increases. For pressure above 8 kbar a three-dimensional metallic phase develops. At lower temperatures charge order and anion order appear subsequently. Both phase boundaries move towards lower temperature with increasing pressure.

4.3. (TMTTF)₂ReO₄

As listed in Table 1, (TMTTF)₂ReO₄ is the compound with the highest CO and AO transition temperatures in the whole family of Fabre salts. At ambient pressure (TMTTF)₂ReO₄ develops CO at $T_{CO} \approx 230$ K and the AO transition at $T_{AO} \approx 160$ K. Figure 14a displays the results of our pressure and temperature-dependent dc resistivity measurements along the perpendicular direction. The corresponding temperature derivative $d\ln\{\rho_c\}/d\left(\frac{1}{T}\right)$ is a measure of the energy gap for activated charge transport; its temperature dependence is presented in Figure 14b. The CO temperature T_{CO} can be identified as a kink in $\rho_c(T, p)$. Even more pronounced is the anion order at T_{AO} .

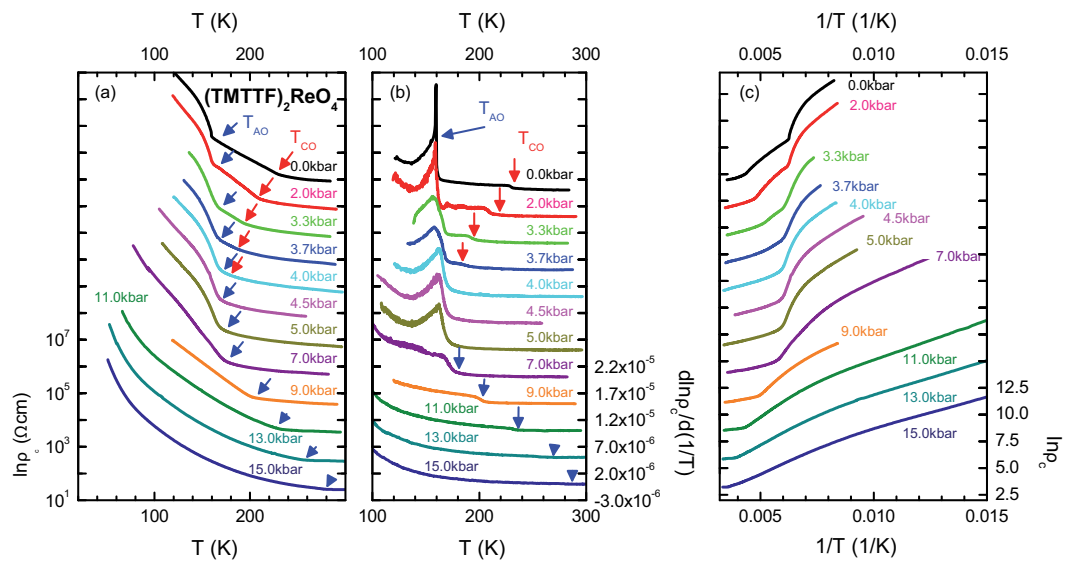


Figure 14. (a) Temperature-dependent resistivity of $(\text{TMTTF})_2\text{ReO}_4$ measured along the c^* -direction for different values of external pressure. The red and black arrows indicate the charge order and anion order transition temperatures. (b) The temperature derivative $d \ln(\rho)/d(1/T)$ shows the charge-order transition as a step in the temperature dependence; the anion ordering T_{AO} is seen as a pronounced peak. Both exhibit a distinct pressure dependence. (c) Arrhenius plot of the resistivity $\rho_c(T)$ as the pressure increases. All curves are shifted with respect to each other for clarity reasons.

For $T < T_{\text{AO}}$ the resistivity increase can be described by an activated behavior with an energy gap that increases in a BCS-like fashion; more details on the dc transport at ambient pressure can be found by Köhler et al. [4]. When hydrostatic pressure is applied, T_{CO} shifts to lower values and resistivity changes at the transition get weaker. T_{AO} on the other hand does not move in temperature for $p < p_{\text{crit}} = 5$ kbar. Also the qualitative shape of $\rho_c(T)$ and its slope for $T \leq T_{\text{AO}}$ do not change significantly in this pressure range. In the derivative of the resistivity, the AO transition appears as a sharp peak, indicating a first-order phase transition for all values $p \leq p_{\text{crit}} = 5.0$ kbar. When the CO transition coincides with the anion ordering, a sudden change in the pressure dependence of T_{AO} is observed. Above a critical pressure $p_{\text{crit}} = 5.0$ kbar the AO related kink moves to higher temperatures when pressure increases further. In addition, the shape of $\rho_c(T)$ changes from a BCS-like to a rather straight and flat evolution of $\rho_c(T)$ for temperatures $T \leq T_{\text{AO}}$. For higher pressures, $p > p_{\text{crit}}$ the shape of the transition resembles a second-order phase transition. The strong reduction of the energy gap Δ at low temperatures for increasing pressures $p > p_{\text{crit}}$ can be seen best in the Arrhenius plot of Figure 14c.

In Figure 15c–e we show the temperature dependence of the charge and anion ordering gaps, Δ_{CO} and Δ_{AO} , respectively, for selected pressures. With increasing pressure $p < p_{\text{crit}}$, the energy gap Δ_{CO} continuously converges to zero at the critical pressure of 5.0 kbar is approached. On the contrary, Δ_{AO} stays fixed. For higher pressure $p > p_{\text{crit}}$, Δ_{AO} gets continuously suppressed as well. For comparison the dc measurements of Coulon et al. [41] along the chain direction, $\rho_a(T, p)$ are presented in Figure 15b. They exhibit qualitatively the same behavior as our dc results in the perpendicular direction.

By extracting the temperatures for the different phase transitions from our resistivity data we can compose a phase diagram of $(\text{TMTTF})_2\text{ReO}_4$ presented in Figure 15a. The CO state is limited to low pressure. Pressure-dependent X-ray investigations may shed light on the origin of the sudden change at the critical pressure of $p_{\text{crit}} \approx 5.0$ kbar. By comparison with the sister compound $(\text{TMTSF})_2\text{ReO}_4$, we can speculate about a change in anion superstructure. As shown in Figure 15f, Moret et al. [62] found a change from $q_2 = (\frac{1}{2}, \frac{1}{2}, \frac{1}{2})$ to $q_3 = (0, \frac{1}{2}, \frac{1}{2})$ superstructure vector as pressure exceeds a certain critical pressure.

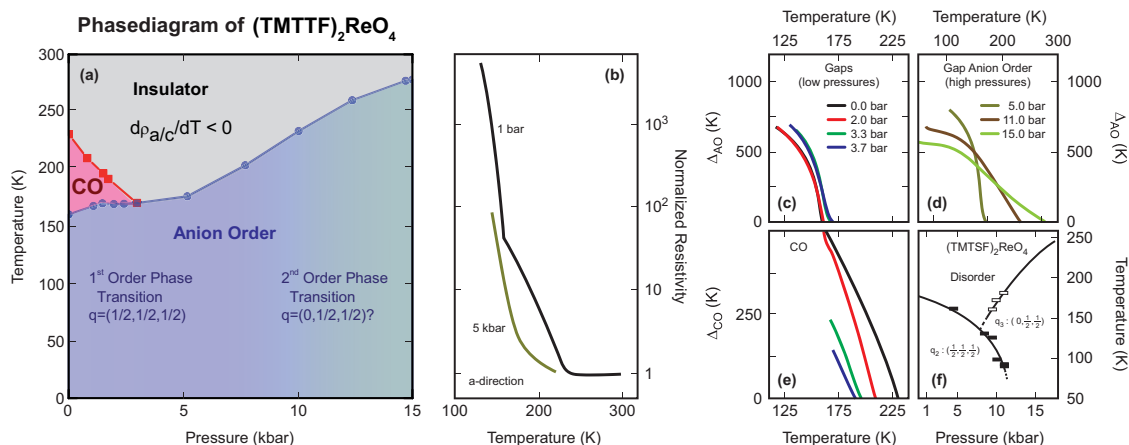


Figure 15. (a) Phase diagram of $(\text{TMTTF})_2\text{ReO}_4$ as obtained from our pressure- and temperature-dependent transport measurements. Even for 15 kbar hydrostatic pressure, no metallic behavior is observed up to room temperature. The charge-ordered phase is limited to low pressure values. The transition into the anion-ordered state changes from first to second order. (b) Normalized dc resistivity versus temperature measured at 1 bar and 5 kbar along the chain direction of $(\text{TMTTF})_2\text{ReO}_4$; reproduced from [41]. (c–e) Temperature change of the activation energy obtained below the AO transition and CO transition of $(\text{TMTTF})_2\text{ReO}_4$ for different pressure. (f) Temperature-dependent anion-ordering phase diagram of $(\text{TMTSF})_2\text{ReO}_4$ as obtained from X-ray scattering experiments of Moret et al. [62]. The q_2 and q_3 phase boundaries overlap at $p = 9.5, 10,$ and 11 kbar and they have opposite slopes.

4.4. Discussion

For a better comparison, in Figure 16 we present next to each other the temperature-dependent resistivity of the three Fabre salts $(\text{TMTTF})_2X$ with tetrahedral anions, $X = \text{BF}_4, \text{ClO}_4,$ and ReO_4 , obtained at different pressure. In the case of centrosymmetric anions a simple relation between anions size and charge ordering could be derived [18]: the larger the anions, the larger the stack separation and the higher T_{CO} . This concept fails for the tetrahedral anions. Obviously the original idea of anions as pure spacers between the one-dimensional TMTTF stacks has to be discarded; instead we have to account for the three-dimensional lattice structure and in particular the interaction of the organic stacks with the anions.

Based on the size of the anions [52], $V_{\text{Anion}}^{\text{BF}_4} < V_{\text{Anion}}^{\text{ClO}_4} < V_{\text{Anion}}^{\text{ReO}_4}$, the CO temperature of $(\text{TMTTF})_2\text{ClO}_4$ should fall right between $T_{\text{CO}}^{\text{BF}_4}$ and $T_{\text{CO}}^{\text{ReO}_4}$. Surprisingly, no CO transition is detected in $(\text{TMTTF})_2\text{ClO}_4$. Provided it is not just an exception to the general rule, $(\text{TMTTF})_2\text{ClO}_4$ may be the key compound for understanding the Fabre salts. Comparing our resistivity data for the three different compounds in Figure 16 reveals that the absence of CO has drastic consequences on the $\rho(T)$ for $T < T_{\text{AO}}$. At ambient pressure no qualitative difference is observed of $X = \text{BF}_4$ and ClO_4 ; at T_{AO} the resistivity exhibits a step to lower values followed by an activated temperature behavior. This common picture changes when pressure is applied. For $(\text{TMTTF})_2\text{BF}_4$ we still find $\rho(T)$ to be thermally activated down to low temperatures. In $(\text{TMTTF})_2\text{ClO}_4$, however, a large minimum in $\rho(T)$ develops for a temperature range of about 30 K. When the pressure has reached $p = 9.3$ kbar, T_{AO} has shifted down by 25 K for $(\text{TMTTF})_2\text{ClO}_4$, while only 6 K in the case of $(\text{TMTTF})_2\text{BF}_4$. The compound $(\text{TMTTF})_2\text{ReO}_4$ does not show any appreciable temperature shift of T_{AO} for pressure up to $p = 5$ kbar; only after $T_{\text{AO}} \approx T_{\text{CO}}$ the AO temperature suddenly starts to move up quite fast with pressure, cf. Figure 15. At this point it is not clear whether this shift is due to the combination of charge and anion order or whether a new superstructure occurs, as in the case of $(\text{TMTSF})_2\text{ReO}_4$ [62]. Ongoing spectroscopic investigations will clarify this point. In $(\text{TMTTF})_2\text{BF}_4$ our data indicate the survival of both CO and AO under pressure. It would be of interest to follow the ordering temperatures to even higher pressure; we speculate that T_{AO} might move up in temperature as soon as it merges with T_{CO} ;

similar to $(\text{TMTTF})_2\text{ReO}_4$. This would underline the competing influence of CO on the AO transition, as suggested by our transport data.

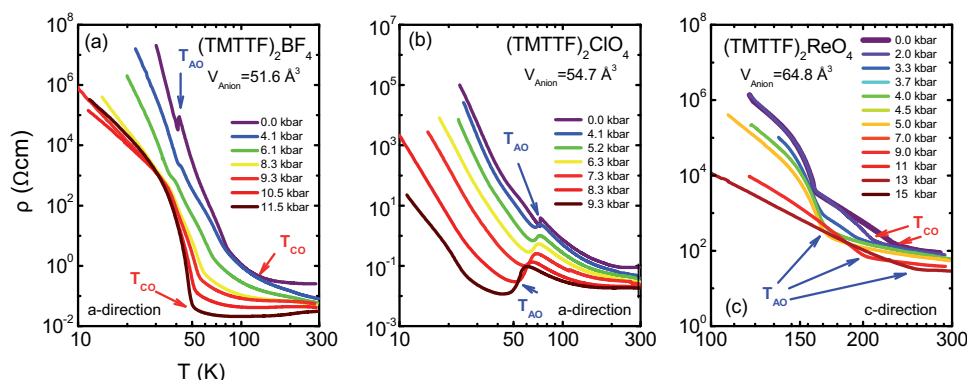


Figure 16. The temperature dependent resistivity for the $(\text{TMTTF})_2\text{X}$ salts with tetrahedral anions. The three compounds are sorted for increasing anion size from left to right. (a) $(\text{TMTTF})_2\text{BF}_4$ is the compound with the smallest anion: $V_{\text{Anion}} = 51.6 \text{ \AA}^3$. It shows both transitions in the dc resistivity, charge and anion ordering. (b) In $(\text{TMTTF})_2\text{ClO}_4$ with $V_{\text{Anion}} = 54.7 \text{ \AA}^3$ only anion ordering was detected but no separate charge order. (c) $(\text{TMTTF})_2\text{ReO}_4$ has by far the largest tetrahedral anion with $V_{\text{Anion}} = 64.8 \text{ \AA}^3$; it also has the highest charge and anion ordering temperatures.

In order to gain further insight into the structural aspects on charge order, Figure 17 displays the distance between the anions and the TMTTF molecule. In the first frame T_{CO} is plotted as a function of the shortest distance between the anion-ligand (F or O) and the sulfur atom on the organic molecule for Fabre salts with tetrahedral as well as octahedral anions. In panel b we consider the distance of the anion center, defined by the B, Cl, Re, P, As or Sb-atoms, to the sulfur atom of the organic molecule. Finally, in Figure 17c we plot the distance of the anion-ligand to the nearest carbon atom. In those cases, T_{CO} behaves differently for $(\text{TMTTF})_2\text{X}$ with octahedral and tetrahedral X. It seems that the distance between the central atom of the anion and the nearest carbon atom reflects the cavity size or the anion size better than any coupling mechanism. The (theoretical) anion volume, listed in Table 1, follows the relation [52]: $V_{\text{Anion}}^{\text{BF}_4} < V_{\text{Anion}}^{\text{ClO}_4} < V_{\text{Anion}}^{\text{ReO}_4} < V_{\text{Anion}}^{\text{PF}_6} < V_{\text{Anion}}^{\text{AsF}_6} < V_{\text{Anion}}^{\text{SbF}_6}$. The correlations plotted in Figure 17 might help to understand some of the effects, but further temperature- and pressure-dependent investigations are needed to completely clarify the situation.

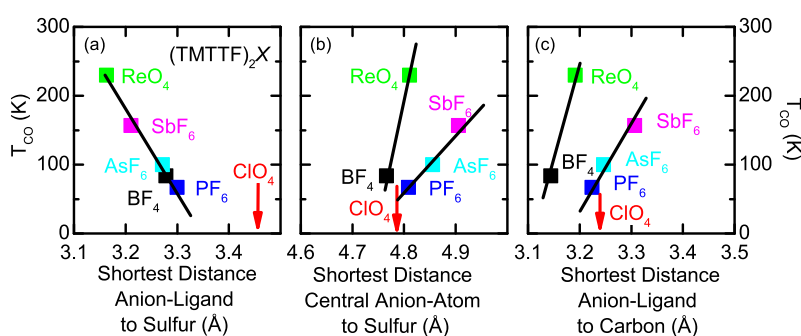


Figure 17. Dependence of the charge order temperature T_{CO} for various Fabre salts $(\text{TMTTF})_2\text{X}$ with different X as indicated. (a) Effect on the shortest distance between anion-ligand and TMTTF sulfur atom. (b) Change of T_{CO} with the distance between the central atom of the anion and the sulfur atom. (c) Influence on the shortest distance from the anion-ligand to the nearest carbon atom. The value for $(\text{TMTTF})_2\text{ClO}_4$, which shows no CO, is indicated by a red arrow. All distances were determined at ambient conditions.

5. Dielectric Spectroscopy

Dielectric spectroscopy is a sensitive tool to detect changes in the charge degrees of freedom that have revealed evidence for CO in the $(\text{TMTTF})_2X$ salts [84,85]. Numerous studies performed over the years [30–36,86] identified a Curie-like peak of the permittivity $\epsilon_a(T)$ at T_{CO} reaching huge values up to 10^6 for $E \parallel a$. While the peak position is frequency-independent up to 1 MHz, its amplitude decreases with rising frequency. The Curie-behavior has drawn a lot of attention [84,85,87–90] because it is characteristic for ferroelectricity. Its origin is considered to be mainly electronic, and thus referred to as “electronic ferroelectricity” [33,91–93]. Nevertheless, the observation of a hysteresis in the electric polarization $P(E)$ is impeded by the high conductivity of the $(\text{TMTTF})_2X$ salts compared with canonical ferroelectrics.

Most of the studies dealt with Fabre salts of centrosymmetric anions, and there is only a single report on $(\text{TMTTF})_2\text{ReO}_4$ and $(\text{TMTTF})_2\text{BF}_4$ [36]. In the first compound, the AO transition is evidenced by a sharp drop of permittivity at T_{AO} ; it is explained by the formation of TMTTF tetramers with a 0110 charge pattern, which are less polarizable compared to dimers [23]. Interestingly, for $(\text{TMTTF})_2\text{BF}_4$ a small peak is revealed at T_{AO} with a frequency-dependent amplitude followed by a monotonous decrease of $\epsilon'_a(T)$ upon further cooling.

5.1. Results

We have conducted frequency-dependent measurements of the real part of the dielectric constant $\hat{\epsilon}_{b'} = \epsilon'_{b'} - i\epsilon''_{b'}$ with the electric field applied perpendicular to the chain direction, $E \parallel b'$, at different temperatures and ambient pressure. The findings for $(\text{TMTTF})_2X$ with $X = \text{BF}_4$, ClO_4 and ReO_4 taken at $f = 1, 10, 100$ kHz, and 1 MHz are plotted in Figure 18. For $(\text{TMTTF})_2\text{BF}_4$ and $(\text{TMTTF})_2\text{ReO}_4$ the charge and anion-order transitions are clearly observed with exactly the same signatures as reported for measurements along the stacking axis [36].

In the case of $(\text{TMTTF})_2\text{BF}_4$, this corresponds to a peak at $T_{\text{CO}} \approx 80$ K, which is reduced in amplitude as frequency increases. For $f = 100$ kHz the peak height of 3000 is lower by factor of 200 compared to a value of $7 \cdot 10^5$ observed for $E \parallel a$ [36]. When the temperature is lowered, $\epsilon'_{b'}(T)$ drops until the AO transition, which is observed here by another peak around 36 K, in accord with the findings for $E \parallel a$. In contrast to the feature T_{CO} , the AO peak is strongly suppressed with increasing frequency. While for $f = 10$ kHz, a value of $\epsilon'_{b'} = 20$ is observed, the peak cannot be identified above 1 MHz.

For the ReO_4 salt, the CO peak appears at 228 K and exhibits a maximum of $4 \cdot 10^4$ when measured at $f = 100$ kHz perpendicular to the chains; this is one order of magnitude lower than the peak found for $E \parallel a$ [36]. With decreasing temperature $\epsilon'_{b'}(T)$ continuously decreases by one order of magnitude at $T_{\text{AO}} = 157$ K, where a step is observed with a frequency-dependent height. Upon further cooling, $\epsilon'_{b'}(T)$ approaches a constant value around 2000, which is slightly dependent on frequency.

$(\text{TMTTF})_2\text{ClO}_4$ exhibits a strong and monotonous decrease in $\epsilon'_{b'}(T)$ from room temperature down to about 100 K. At T_{AO} an abrupt step with a frequency-independent height up to 50 marks the anion order. At lower temperatures $\epsilon'_{b'}(T)$ changes in shape forming a shoulder-like drop of one order of magnitude. Interestingly, for higher frequencies this drop occurs at higher temperatures reminiscent of a dielectric relaxation.

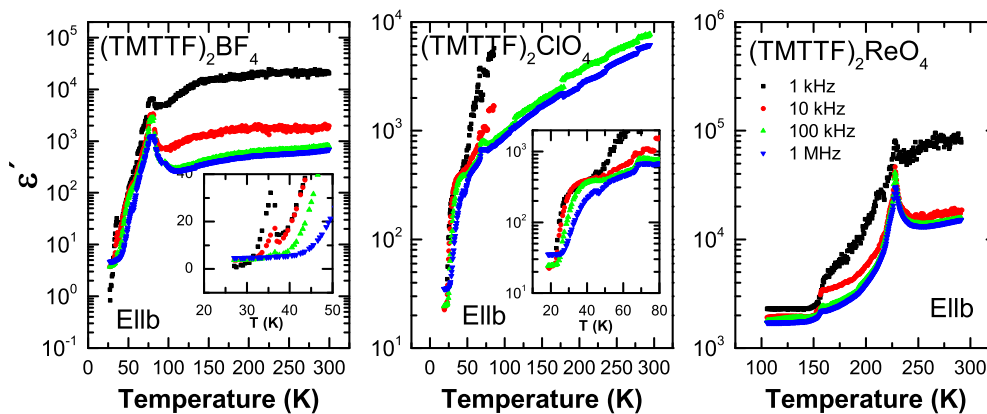


Figure 18. Temperature dependence of the real part of the dielectric permittivity $\epsilon'(T)$ measured with $E \parallel b'$ for $(\text{TMTTF})_2X$ with $X = \text{BF}_4, \text{ClO}_4$ and ReO_4 at different frequencies as indicated. The insets emphasize the changes close T_{AO} and below.

5.2. Analysis

In general, a ferroelectric phase transition is accompanied by a soft mode strongly slowing down near the critical temperature. It is usually observed in optical, infrared or microwave spectroscopy for a displacive phase transition; or by a relaxation mode at lower frequencies, as seen in disordered systems [94,95]. Hence, investigating the relaxation time can provide valuable insight into the dynamics related to the transitions. The Cole-Cole or generalized Debye model is a well established and useful description to analyze the frequency-dependent complex permittivity

$$\hat{\epsilon}(\omega) - \epsilon_{\text{inf}} = \frac{\Delta\epsilon}{1 + (i\omega\tau_0)^{1-\alpha}} \quad (1)$$

where τ_0 is the relaxation time, $\omega = 2\pi f$ the angular frequency of the applied electric ac-field, $1 - \alpha$ a parameter describing symmetric broadening of the loss peak and $\Delta\epsilon = \epsilon_{\text{static}} - \epsilon_{\text{inf}}$ the dielectric strength with ϵ_{static} and ϵ_{inf} the values for low and high frequencies, respectively. The deviation from the Debye model ($\alpha = 0$) is attributed to the distribution of τ_0 arising from disorder [84]. If the materials are not completely insulating, but exhibit a considerable electronic background, such as the $(\text{TMTTF})_2X$ salts, the dc-conductivity has to be taken into account when the dielectric loss is determined:

$$\epsilon''(\omega) = \frac{\sigma'(\omega) - \sigma_{\text{DC}}}{\omega\epsilon_0} \quad (2)$$

As an example for $(\text{TMTTF})_2X$ salts with tetrahedral anions investigated here, Figure 19 shows the dielectric spectra of $(\text{TMTTF})_2\text{ClO}_4$ in the range of the relaxational mode for different temperatures close to the AO transition. The real part of the dielectric constant $\epsilon'_{b'}(\omega)$ is plotted in the upper panel: with increasing frequency it exhibits a step that shift towards higher frequencies as the temperature increases. The point of inflection marks the relaxation rate $1/\tau_0$ and corresponds to the maximum of the broad peak in the imaginary part $\epsilon''_{b'}(\omega)$. The solid lines represent fits according to Equation (1) and agree well with the expected behavior.

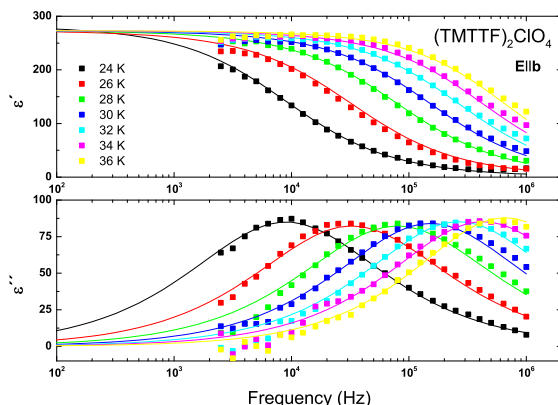


Figure 19. Frequency dependence of the permittivity $\hat{\epsilon}(\omega) = \epsilon'(\omega) - i\epsilon''(\omega)$ of $(\text{TMTTF})_2\text{ClO}_4$ measured with $E \parallel b'$ at various temperatures close to the AO transition. The real part $\epsilon'(\omega)$ exhibits a roll-off that shifts to higher frequencies with increasing temperature. This behavior corresponds to a peak in $\epsilon''(\omega)$ as shown in the lower panel. The solid lines represent fits according to the generalized Debye model (1).

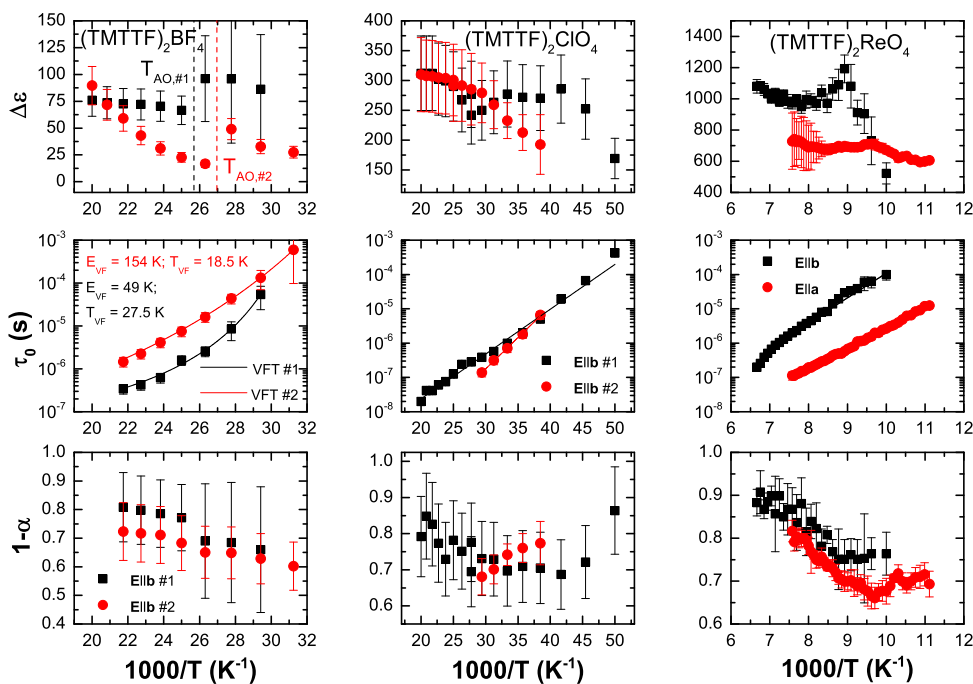


Figure 20. Temperature dependence of the parameters used to fit the dielectric spectra of $(\text{TMTTF})_2\text{BF}_4$, $(\text{TMTTF})_2\text{ClO}_4$ and $(\text{TMTTF})_2\text{ReO}_4$ by the Cole-Cole model (1). The upper row shows the Arrhenius plots of the dielectric strength $\Delta\epsilon$, followed by the relaxation time τ_0 and the broadening parameter $(1 - \alpha)$ in the lower row. For $X = \text{BF}_4$ and ClO_4 the data on two crystals each (indicated by black and red symbols) are taken for $E \parallel b'$. For $X = \text{ReO}_4$ we show data measured along the a and b' -directions. Most important, in $(\text{TMTTF})_2\text{ClO}_4$ and $(\text{TMTTF})_2\text{ReO}_4$ the relaxation time τ_0 exhibits an activated behavior; the obtained activation energies resembles the gap previously measured in dc transport [4]. For $(\text{TMTTF})_2\text{BF}_4$, $\tau_0(T)$ increases with decreasing T in a fashion best described by the empirical Vogel-Fulcher-Tammann relation.

The parameters $\Delta\epsilon$, τ_0 and $1 - \alpha$ extracted from the Cole-Cole fit of the dielectric spectra are plotted in Figure 20 as a function of inverse temperature. The data have been recorded along the b' direction of the $(\text{TMTTF})_2\text{BF}_4$, $(\text{TMTTF})_2\text{ClO}_4$ and $(\text{TMTTF})_2\text{ReO}_4$ salts. We confined ourselves to this temperature region because our experimental frequency window is restricted to 1 MHz. For $(\text{TMTTF})_2\text{BF}_4$ the

relaxation mode moves through this frequency window for $50 \text{ K} > T > 30 \text{ K}$, which includes the AO transition. Here $\Delta\epsilon$ exhibits a small peak around $T = 38 \text{ K}$ and 36 K for the two different samples, labeled 1 (black) and 2 (red symbols). These steps correspond to the features observed in $\hat{\epsilon}(T)$ (Figure 18) and are ascribed to the AO transition. The broadening parameter $(1 - \alpha)$ decreases upon cooling indicating an increased cooperativity in the relaxation. Interestingly, $\tau_0(T)$ rises with lowering temperature in a fashion best described by the empirical Vogel-Fulcher-Tammann relation

$$\tau_0 = \tau_{\text{VF}} \exp \left\{ \frac{E_{\text{VF}}}{T - T_{\text{VF}}} \right\} , \quad (3)$$

which is known as a good parametrization for the slowing down of molecular motion in disordered systems and the glass-like freezing of dipolar order in relaxor ferroelectrics. The corresponding energy E_{VF} can be interpreted as a temperature-dependent activation energy for reorientational motion. T_{VF} denotes the temperature where τ_0 diverges, and τ_{VF} the time scale for the ac response in the high-temperature limit. The glass temperature T_G is defined as the temperature where $\tau_0 = 100 \text{ s}$. The obtained fit parameters are listed in Table 2. There is a considerable difference in the values for E_{VF} and τ_{VF} , whereas there is a minor deviation for T_G which we attribute to different cooling rates during the measurements.

Table 2. Parameters obtained by fitting the temperature-dependent dielectric relaxation time $\tau_0(T)$ of $(\text{TMTTF})_2\text{BF}_4$ with the Vogel-Fulcher-Tammann relation. E_{VF} is the activation energy, T_{VF} denotes the Vogel-Fulcher temperature, and τ_{VF} the corresponding time scale. The glass temperature is given by T_G .

$(\text{TMTTF})_2\text{BF}_4$	Sample 1	Sample 2
E_{VF} (K)	49 ± 7	153.5 ± 11.5
T_{VF} (K)	27.5 ± 0.5	18.5 ± 0.5
τ_{VF} (s)	$(2.5 \pm 1.2) \cdot 10^{-8}$	$(6.1 \pm 2.5) \cdot 10^{-9}$
T_G (K)	30	25

For $(\text{TMTTF})_2\text{ClO}_4$ the mode can be observed in our frequency window between $T = 20 \text{ K}$ and 50 K , which is below T_{AO} , but in the range of the dispersive shoulder-like drop in $\epsilon'_{b'}(T)$ shown in Figure 18. For the second crystal, we observe a monotonous decrease of $\Delta\epsilon$ with falling temperature, in agreement with the behavior of $\epsilon'_{b'}(T)$. There is an additional small bump around $T = 23 \text{ K}$ for sample 1. In both specimens an activated behavior in τ_0 is observed with activation energies of 300 K and 420 K , respectively. The fit parameters are listed in Table 3. We can compare our findings with the energy gap of $(440 \pm 60) \text{ K}$ derived from dc-transport measurements reported in Reference [4].

Table 3. Parameters of the activated behavior of τ_0 for $(\text{TMTTF})_2\text{ClO}_4$ derived from dielectric measurements of two different crystals.

$(\text{TMTTF})_2\text{ClO}_4$	Sample 1	Sample 2
E_{act} (K)	300 ± 10	420 ± 8
τ_{act} (s)	$(5.7 \pm 1.9) \cdot 10^{-11}$	$(6.0 \pm 1.7) \cdot 10^{-13}$

The relaxation mode in $(\text{TMTTF})_2\text{ReO}_4$ slows down more quickly; it enters our experimental frequency window for $90 \text{ K} < T < 140 \text{ K}$, right below the AO transition. Surprisingly, there is a small peak in $\Delta\epsilon$ at $T = 112$ and 105 K for $E \parallel b'$ and $E \parallel a$, respectively, which superimposes a gradual increase with temperature. No corresponding counterpart is observed in $\epsilon'_{b'}(T)$. For both directions, τ_0 follows an activated behavior; the fit parameters are listed in Table 4 for the two polarization directions.

From dc transport a temperature-dependent energy gap was derived [4] that saturates at (1560 ± 80) K in the limit of $T \rightarrow 0$ for all crystal directions.

Table 4. Parameters of the activated behavior observed in τ_0 for two crystal directions of $(\text{TMTTF})_2\text{ReO}_4$.

$(\text{TMTTF})_2\text{ReO}_4$	$E \parallel a$	$E \parallel b'$
E_{act} (K)	1372 ± 4	1651 ± 27
τ_{act} (s)	$(3.1 \pm 0.1) \cdot 10^{-12}$	$(7.3 \pm 1.6) \cdot 10^{-12}$

Since for $(\text{TMTTF})_2\text{ClO}_4$ and $(\text{TMTTF})_2\text{ReO}_4$ the activation energies of the relaxation time τ_0 agree well with the values obtained by dc-transport, we conclude that the relaxation is determined by the free charge carries responsible for the dc conduction, which freeze out at low temperatures.

5.3. Discussion

For the $(\text{TMTTF})_2X$ salts, the peak in ϵ' at T_{CO} obeys Curie's law as established for canonical order-disorder ferroelectrics [84]; it is attributed to a combination of charge disproportionation and ionic displacements [32,33].

As far as the anisotropy is concerned, the ratio of the peak amplitudes $\epsilon'_a/\epsilon'_{b'}$ probed at $f = 100$ kHz is about 200 and 1000 for $(\text{TMTTF})_2\text{BF}_4$ and $(\text{TMTTF})_2\text{ReO}_4$, respectively, higher than the anisotropy of the dc resistivity at T_{CO} [4]. It is interesting to compare our findings with the report of de Souza et al. [96] on the Fabre salts with octahedral anions. As reproduced in Figure 21, they found a strong peak in ϵ'_c at T_{CO} similar to previous reports on $\epsilon'_a(T)$ [30–32,34–36] and $\epsilon'_{b'}(T)$ presented here (Figure 18). The peak value is sample-dependent and in general by several orders of magnitude lower compared the value observed along the stacks. While in the a -direction the permittivity is affected by critical fluctuations that become important when approaching the ordering transition in one dimension, the response in the perpendicular direction probes the involvement of ionic displacements and the stabilization of the three-dimensional charge pattern upon CO.

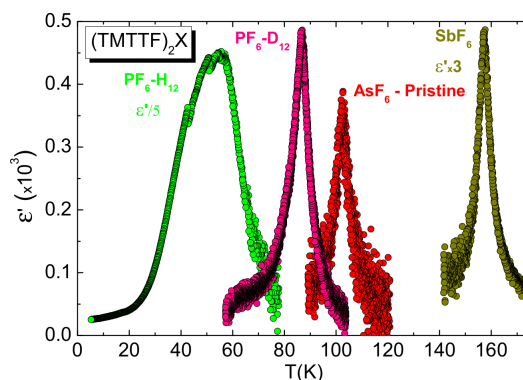


Figure 21. Temperature dependence of the dielectric constant of several $(\text{TMTTF})_2X$ salts with octahedral anions: H_{12} - $(\text{TMTTF})_2\text{PF}_6$ and D_{12} - $(\text{TMTTF})_2\text{PF}_6$, $(\text{TMTTF})_2\text{AsF}_6$ and $(\text{TMTTF})_2\text{SbF}_6$. The experiments have been performed along the c^* -axis perpendicular to the chain direction [96]. The maximum in $\epsilon'_c(T)$ is located at T_{CO} , similar to measurements along the other orientations $\epsilon'_a(T)$ [30–32,34–36] and $\epsilon'_{b'}(T)$. The peak value is lower by several orders of magnitude compared to ϵ'_a , similar to the anisotropy determined in dc transport [4].

The rather high values of $\epsilon'(T)$ at room temperature, found in Figure 18, are attributed to the slight dimerization of the TMTTF molecules and the resulting enhanced polarizability, which scales with $\epsilon' \approx (\omega_p/\Delta)^2$, wherein ω_p is the plasma frequency and Δ the transport gap [97]. The temperature dependence of $\Delta(T)$ for $E \parallel b'$ is found [4] constant for $(\text{TMTTF})_2\text{ReO}_4$ from $T = 300$ K to 250 K,

whereas it is decreasing for $(\text{TMTTF})_2\text{ClO}_4$ and $(\text{TMTTF})_2\text{BF}_4$; the latter is explained by the decrease in dimerization. Accordingly, the reduction of $\epsilon'_b(T)$ upon cooling observed here is induced by the decrease of $\omega_p(T)$ due to the freezing out of mobile charge carriers. This can be confirmed by detailed optical investigation of all $(\text{TMTTF})_2X$ salts.

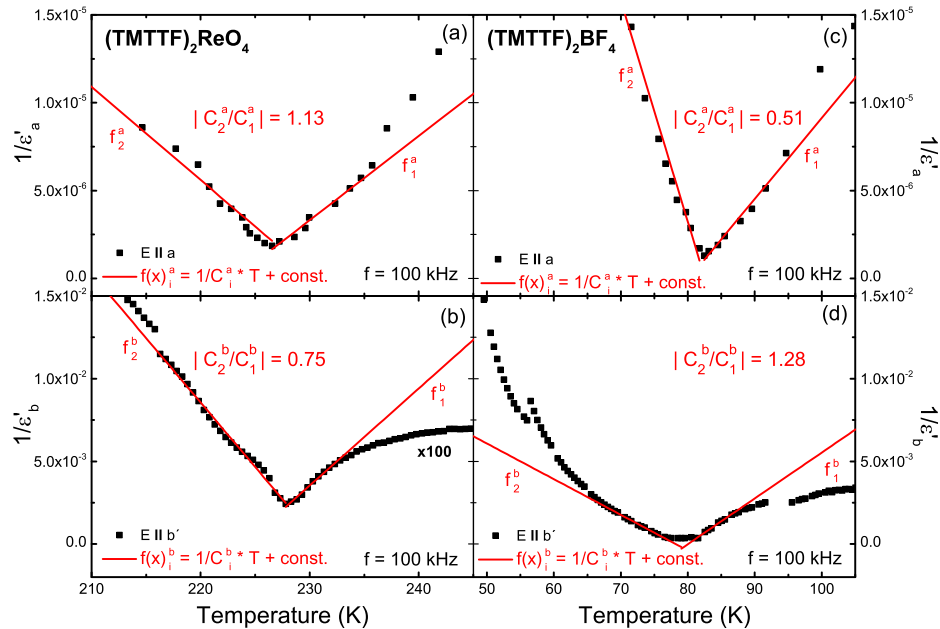


Figure 22. Temperature dependence of (a,c) $1/\epsilon'_a(T)$ (data from [36]) and (b,d) $1/\epsilon'_b(T)$ for (a,c) $(\text{TMTTF})_2\text{BF}_4$ and (b,d) $(\text{TMTTF})_2\text{ReO}_4$. There is good agreement with the Curie-Weiss behavior (red solid lines) for $T \leq T_{\text{CO}}$, except for $(\text{TMTTF})_2\text{BF}_4$ along b' -direction, where the peak in $\epsilon'_b(T)$ is somewhat rounded. For canonical second-order ferroelectric transitions, mean-field theory predicts that the slopes on both side differ by a factor of 2 [94]. The deviation from this expected behavior is usually attributed to structural disorder [36,86].

The Curie-Weiss behavior $\epsilon'(T) = \frac{C}{T-T_{\text{CO}}}$ is nicely illustrated in Figure 22 where $1/\epsilon'_a(T)$ and $1/\epsilon'_b(T)$ are plotted for $(\text{TMTTF})_2\text{BF}_4$ and $(\text{TMTTF})_2\text{ReO}_4$. In particular for $T \leq T_{\text{CO}}$ the agreement is rather good, except for $(\text{TMTTF})_2\text{BF}_4$ along the b' -direction (cf. Figure 18). Above T_{CO} we observe rather large deviations from the expected behavior for both salts.

At this point it is important to mention that the amplitude and broadening of the CO peak in $\epsilon'_a(T)$ is known to be sample-dependent [36,86] and hence, in case a deviation from the Curie-behavior is observed below T_{CO} , it is ascribed to structural disorder. The latter also explains, why the slope ratio $|C_2^{a,b}/C_1^{a,b}|$ deviates in some reports [86,96] from the expected value 0.5, which is predicted by mean field theory for a canonical second-order phase transition [94].

The ratio of the slope obtained along the b' -direction does not necessarily infer a minor sample quality. The CO peak is weaker along the b' -direction, implying that at high temperatures the contribution of dimerization to the background could be appreciable. Similar deviations from this mean-field dependence are observed for $(\text{TMTTF})_2\text{AsF}_6$ and $(\text{TMTTF})_2\text{PF}_6$ when looking along the c^* -direction [96]. Additional ionic contributions are more pronounced in the perpendicular polarizations and should be investigated in more detail in future.

For $(\text{TMTTF})_2\text{ReO}_4$ the abrupt drop of the permittivity at T_{AO} evidences the formation of TMTTF tetramers with a 0110 charge pattern; they are less polarizable compared to dimers. Interestingly, in $(\text{TMTTF})_2\text{BF}_4$ a small peak is observed at T_{AO} , followed by the drop due to tetramerization. The absence of a comparable peak in the other two salts may be due to screening by free charge carriers. In $(\text{TMTTF})_2\text{BF}_4$ the resistivity at T_{AO} is three orders of magnitudes higher compared to $(\text{TMTTF})_2\text{ReO}_4$, for instance [4]. In the case of $(\text{TMTTF})_2\text{ClO}_4$ there is no CO for $T > T_{\text{AO}}$. Below T_{AO} , around $T = 50$ K,

there is a second drop which shifts to higher temperature for increasing frequency, reminiscent of a dielectric relaxation. Note that in this temperature range, ESR measurements reveal a drop of the spin susceptibility [73], which is attributed to the formation of a spin singlet-triplet gap upon tetramerization, and optical investigations [23] prove the growth of charge disproportionation with a 0110 charge pattern. Further investigations have to fully clarify the connection to the observed dielectric relaxation. The observation of a corresponding feature in $(\text{TMTTF})_2\text{BF}_4$ and $(\text{TMTTF})_2\text{ReO}_4$ might be obscured by a strong background due to the CO peak.

In $(\text{TMTTF})_2\text{AsF}_6$ the mean relaxation time $\tau_0(T)$ contains a peak at T_{CO} due to the softening of the oscillating mode concomitant to the ferroelectric transition and an activated behavior with an activation energy similar to the gap obtained by dc transport [35,86]. Brazovskii and coworkers [89] report an additional relaxation mode in $(\text{TMTTF})_2\text{AsF}_6$ for $T < T_{\text{CO}}$, which is ascribed to slow oscillations of pinned ferroelectric domains. Recent Raman spectroscopy evidences the presence of neutral TMTTF^0 and ionized TMTTF^{-1} molecules, which are assigned to charged domain walls [56]. It is worthwhile to mention that in the two-dimensional charge-transfer salts $\kappa\text{-(BEDT-TTF)}_2\text{X}$, with $\text{X} = \text{Cu}[\text{N}(\text{CN})_2]\text{Cl}$ [98], $\text{Cu}_2(\text{CN})_3$ [99,100] and $\text{Ag}_2(\text{CN})_3$ [101], as well as in $\alpha\text{-(BEDT-TTF)}_2\text{I}_3$ [102,103], charge domain walls are also considered to give rise to an anomalous dielectric response in the audio- and radio-frequency range. For $(\text{TMTTF})_2\text{ClO}_4$ and $(\text{TMTTF})_2\text{ReO}_4$ the activation energies of the relaxation time $\tau_0(T)$ agree well with dc-transport measurements, in accord with the observations for $(\text{TMTTF})_2\text{PF}_6$ [31] and $(\text{TMTTF})_2\text{AsF}_6$ [35,86]. This indicates that the relaxation is determined by the free charge carriers responsible for the dc-conduction, which freeze out at low temperatures. We assume that crystal defects and charged impurities locally change the charge pattern due to anion order, giving rise to domains walls. If charge carriers are thermally activated above the transport gap, which is composed of the contributions due to dimerization, charge and anion order [4], they move along the TMTTF chains adding to the dc-conductivity. This changes the charge pattern and results in an effective shift of the domain walls, explaining why the activation energy of the relaxation time corresponds to the dc-transport gap.

For $(\text{TMTTF})_2\text{BF}_4$ with $T_{\text{AO}} = 41.5$ K, the relaxation mode is observed for $50 \text{ K} > T > 30 \text{ K}$ and the relaxation time $\tau_0(T)$ follows the empirical Vogel-Fulcher-Tammann relation. In this temperature range, the resistivity is rather high and transport is ascribed to hopping conduction [4]. The drastic decreased number of free charge carriers results in glass-like freezing of domain walls, as evidenced by the observation of the Vogel-Fulcher behavior. Surprisingly, the results obtained here for $T < T_{\text{AO}}$ on the salts with tetrahedral anions agree well with the ones obtained for $T < T_{\text{CO}}$ on the centrosymmetric anions, indicating that the underlying order determining the charge pattern is of minor role for the relaxation dynamics.

6. Conclusions

Our pressure-dependent DC-transport measurements yield valuable information on the influence of the lattice on the ordering phenomena in the quasi one-dimensional charge-transfer salts $(\text{TMTTF})_2\text{X}$ with tetrahedral anions $\text{X} = \text{BF}_4$, ClO_4 and ReO_4 . We observe a decrease of the charge ordering temperature T_{CO} upon pressure for $(\text{TMTTF})_2\text{BF}_4$ and $(\text{TMTTF})_2\text{ReO}_4$; similar to the observation reported for salts with octahedral anions [104]. In contrast to CO, the pressure dependence of AO differs for each salt such that the construction of a generic phase diagram of $(\text{TMTTF})_2\text{X}$ salts with tetrahedral anions is not possible. In $(\text{TMTTF})_2\text{BF}_4$, CO is visible up to the highest pressure applied with $T_{\text{CO}}(p = 8.8 \text{ kbar}) = 47.5$ K whereas the signature indicating AO dissolves around 34.5 K at a pressure of 5.3 kbar. We call for structural studies that will yield information on the actual arrangement of the anions. In $(\text{TMTTF})_2\text{ReO}_4$, AO is enhanced upon applying pressure with an increase of T_{AO} , at around 3.0 kbar $T_{\text{AO}} = T_{\text{CO}}$ is reached and for pressures above, CO seems to be fully suppressed and the AO shifted up to 277 K at $p = 14.7$ kbar. Interestingly in $(\text{TMTTF})_2\text{ClO}_4$, the jump-like feature indicating AO shifts to lower temperatures and significantly broadens. For $p > 10.2$ kbar, we observe a second peak evolving right at T_{AO} whose origin is still unclear. The fact that no CO is detected in

(TMTTF)₂ClO₄ is probably the most puzzling observation that calls for explanation. We attribute the absence of CO in (TMTTF)₂ClO₄ to the polarizability of the anion. ClO₄ is less polarizable because Cl has an electronegativity comparable to O. Consequently, the bonds within the anion are more covalent making the anion more stiff and less deformable. As a result, the ClO₄ adapts less to the methyl cavity and deforms them more strongly. The deformation leads to a change of the π -orbital direction, which – considering one particular anion stack – applies to every second TMTTF molecule of a neighboring stack. This modulates the direction of the transfer integrals for every second TMTTF molecule and results in an increased value of the electronic dimerization δ_{elec} (cf. Table 1), preventing the emergence of CO in (TMTTF)₂ClO₄.

We furthermore performed measurements of the permittivity along b' direction, perpendicular to the stacking, and observe qualitatively the same signatures in $\epsilon'_{b'}$ as in literature for ϵ'_a . The ratio of the peak amplitudes $\epsilon'_a/\epsilon'_{b'}$ at 100 kHz is 200 and 1000 for (TMTTF)₂BF₄ and (TMTTF)₂ReO₄, respectively, are higher than the anisotropy at T_{CO} determined by dc resistivity measurements [4]. This reflects the one-dimensional nature of the critical fluctuations when approaching T_{CO} , whereas the reduced value along the b' -direction is due to the displacement of anions upon formation of the three-dimensional charge pattern. For all salts investigated, an abrupt drop of the permittivity at T_{AO} is detected, which is attributed to the formation of TMTTF tetramers with 0110 charge pattern. By analyzing the frequency dependence of ϵ_b , we observe a dielectric relaxation below T_{AO} . In (TMTTF)₂ClO₄ and (TMTTF)₂ReO₄, we observe an activated behavior of the relaxation time with activation energies resembling the gap measured in transport, indicating that the relaxation dynamics are determined by free charge carriers. This agrees quite well with observations in (TMTTF)₂PF₆ [31] and (TMTTF)₂AsF₆ [35,86] for $T < T_{CO}$, for which the relaxation time is activated and corresponding activation energies match to the dc-transport gap as well. This indicates that the relaxation is determined by the free charge carriers responsible for the dc conduction which freeze out at low temperatures and that the underlying order giving rise to the transport gap plays a minor role.

Acknowledgments: We appreciate financial support by the Deutsche Forschungsgemeinschaft (DFG) and Deutsche Akademischer Austauschdienst (DAAD).

Author Contributions: E.R. and K.S. conducted the pressure-dependent transport experiments, T.B., M.G., E.R. and T.I. performed the dielectric measurements, R.R., E.R. and A.P. contributed to the data analysis, R.R., E.R. and M.D. wrote the paper; all authors contributed to the discussion.

Conflicts of Interest: Declare conflicts of interest or state The authors declare no conflict of interest.

Abbreviations

The following abbreviations are used in this manuscript:

TMTTF	tetramethyltetrafulvalene
TMTSF	tetramethyltetraselenafulvalene
CO	charge ordering
AO	anion ordering
NEXAFS	X-ray absorption near edge structure
NMR	nuclear magnetic resonance
ESR	electron spin resonance
DFT	density functional theory

References

1. Giamarchi, T. *Quantum Physics in One Dimension*; Clarendon Press: Oxford, UK, 2004.
2. Dressel, M. Spin-charge separation in quasi one-dimensional organic conductors. *Naturwissenschaften* **2003**, *90*, 337–344.
3. Dressel, M. Ordering phenomena in quasi-one-dimensional organic conductors. *Naturwissenschaften* **2007**, *94*, 527–541.

4. Köhler, B.; Rose, E.; Dumm, M.; Untereiner, G.; Dressel, M. Comprehensive transport study of anisotropy and ordering phenomena in quasi-one-dimensional (TMTTF)₂X salts (X=PF₆, AsF₆, SbF₆, BF₄, ClO₄, ReO₄). *Phys. Rev. B* **2011**, *84*, 035124.
5. Dressel, M.; Hesse, P.; Kirchner, S.; Untereiner, G.; Dumm, M.; Hemberger, J.; Loidl, A.; Montgomery, L. Charge and spin dynamics of TMTSF and TMTTF salts. *Synth. Met.* **2001**, *120*, 719–720.
6. Seo, H.; Hotta, C.; Fukuyama, H. Toward systematic understanding of diversity of electronic properties in low-dimensional molecular solids. *Chem. Rev.* **2004**, *104*, 5005–5036.
7. Jérôme, D. The physics of organic conductors. *Science* **1991**, *252*, 1509–1514.
8. Granier, T.; Gallois, B.; Ducasse, L.; Fritsch, A.; Filhol, A. 4 K crystallographic and electronic structures of (TMTTF)₂X salts (X⁻: PF₆⁻, AsF₆⁻). *Synth. Met.* **1988**, *24*, 343–356.
9. Iwase, F.; Sugiura, K.; Furukawa, K.; Nakamura, T. Electronic properties of a TMTTF-Family Salt, (TMTTF)₂TaF₆: New member located on the *modified* generalized phase-diagram. *J. Phys. Soc. Jpn.* **2009**, *78*, 104717.
10. Liautard, P.B.; Peytavin, S.; Brun, G.M.M. Etude structurale du nitrate de tétraméthyltétrathiafulvalène (TMTTF)₂NO₃. *Acta Cryst. B* **1982**, *38*, 2746–2749.
11. Kobayashi, H.; Kobayashi, A.; Sasaki, Y.; Saito, G.; Inokuchi, H. The crystal structure of (TMTTF)₂ReO₄. *Bull. Chem. Soc. Jpn.* **1984**, 2025–2026.
12. Galigné, J.L.; Liautard, B.; Peytavin, S.; Brun, G.; Maurin, M.; Fabre, J.M.; Torreilles, E.; Giral, L. Structure cristalline du fluoroborate de tetramethyltetrathiafulvalene (TMTTF)₂BF₄ a 100 K et a temperature ambiante. *Acta Cryst. B* **1979**, *35*, 1129–1135.
13. Liautard, P.B.; Peytavin, S.; Brun, G. Structure du di(tétraméthyltétrathiafulvalénium)* perchlorate [(TMTTF)₂ClO₄], 2C₁₀H₁₂S₄^{0.5}.ClO₄⁻. *Acta Cryst. C* **1984**, *40*, 1023–1026.
14. Liautard, P.B.; Peytavin, S.; Brun, G.; Maurin, M. Structural correlations in the series (TMTTF)₂X. *J. Phys.* **1982**, *43*, 1453–1459.
15. Nogami, Y.; Ito, T.; Yamamoto, K.; Irie, N.; Horita, S.; Kambe, T.; Nagao, N.; Shima, K.; Ikeda, N.; Nakamura, T. X-ray structural study of charge and anion orderings of TMTTF salts. *J. Phys. IV* **2005**, *131*, 39.
16. Pouget, J.P.; Ravy, S. Structural aspects of the Bechgaard salts and related Compounds. *J. Phys. I* **1996**, *6*, 1501–1525.
17. Pouget, J.P. Structural aspects of the Bechgaard and Fabre salts: An update. *Crystals* **2012**, *2*, 466–520.
18. Rose, E.; Dressel, M. Coupling between molecular chains and anions in (TMTTF)₂X salts. *Physica B* **2012**, *407*, 1787–1792.
19. Kistenmacher, T.J. Anion-donor coupling in (TMTSF)₂X salts: Symmetry considerations. *Solid State Commun.* **1984**, *51*, 931–934.
20. Liautard, P.B.; Peytavin, S.; Brun, G.; Maurin, M. Structural studies and physical properties in the organic conductors series (TMTTF)₂X and (TMTSF)₂X. *J. Phys.* **1983**, *44*, C3-951–C3-956.
21. Kistenmacher, T.J. Cavity size versus anion size in (TMTSF)₂X salts: Possible implications for the uniqueness of (TMTSF)₂ClO₄. *Solid State Commun.* **1984**, *50*, 729–733.
22. Thorup, N.; Rindorf, G.; Soling, H.; Bechgaard, K. The structure of di(2,3,6,7-tetramethyl-1,4,5,8-tetrathiafulvalenium hexafluorophosphate, (TMTSF)₂PF₆, the first superconducting organic solid. *Acta Cryst. B* **1981**, *37*, 1236–1240.
23. Pustogow, A.; Peterseim, T.; Kolatschek, S.; Engel, L.; Dressel, M. Electronic correlations versus lattice interactions: Interplay of charge and anion orders in (TMTTF)₂X. *Phys. Rev. B* **2016**, *94*, 195125.
24. Coulon, C.; Delhaes, P.; Flandrois, S.; Lagnier, R.; Bonjour, E.; Fabre, J.M. A new survey of the physical properties of the (TMTTF)₂X series. Role of the counterion ordering. *J. Phys.* **1982**, *43*, 1059–1067.
25. Beno, M.A.; Blackman, G.S.; Leung, P.C.W.; Williams, J.M. Hydrogen bond formation and anion ordering in superconducting (TMTSF)₂ClO₄ and (TMTSF)₂AsF₆. *Solid State Commun.* **1983**, *48*, 99–103.
26. Granier, T.; Gallois, B.; Fritsch, A.; Ducasse, L.; Coulon, C. 135 K crystallographic and electronic structure of (TMTTF)₂SbF₆. In *Lower-Dimensional Systems and Molecular Electronics*; Metzger, R.M., Day, P., Papavassiliou, G.C., Eds.; Springer: Boston, MA, USA, 1990; Volume 248, pp. 163–168.
27. Subías, G.; Abbaz, T.; Fabre, J.M.; Fraxedas, J. Characterization of the anion-ordering transition in (TMTTF)₂ReO₄ by X-ray absorption and photoemission spectroscopies. *Phys. Rev. B* **2007**, *76*, 085103.
28. Chow, D.S.; Zamborszky, F.; Alavi, B.; Tantillo, D.J.; Baur, A.; Merlic, C.A.; Brown, S.E. Charge ordering in the TMTTF family of molecular conductors. *Phys. Rev. Lett.* **2000**, *85*, 1698–1701.

29. Zamborszky, F.; Yu, W.; Raas, W.; Brown, S.E.; Alavi, B.; Merlic, C.A.; Baur, A. Competition and coexistence of bond and charge orders in $(\text{TMTTF})_2\text{AsF}_6$. *Phys. Rev. B* **2002**, *66*, 081103.
30. Nad, F.; Monceau, P.; Carcel, C.; Fabre, J.M. Charge ordering phase transition in the quasi-one-dimensional conductor $(\text{TMTTF})_2\text{AsF}_6$. *J. Phys. Condens. Matter* **2000**, *12*, L435–L440.
31. Nad, F.; Monceau, P.; Carcel, C.; Fabre, J.M. Dielectric response of the charge-induced correlated state in the quasi-one-dimensional conductor $(\text{TMTTF})_2\text{PF}_6$. *Phys. Rev. B* **2000**, *62*, 1753.
32. Nad, F.; Monceau, P.; Carcel, C.; Fabre, J.M. Charge and anion ordering phase transitions in $(\text{TMTTF})_2\text{X}$ salt conductors. *J. Phys. Condens. Matter* **2001**, *13*, L717–L722.
33. Monceau, P.; Nad, F.Y.; Brazovskii, S. Ferroelectric Mott-Hubbard phase of organic $(\text{TMTTF})_2\text{X}$ conductors. *Phys. Rev. Lett.* **2001**, *86*, 4080–4083.
34. Nagasawa, M.; Nad, F.; Monceau, P.; Fabre, J.M. Modification of the charge ordering transition in the quasi-one-dimensional conductor $(\text{TMTTF})_2\text{SbF}_6$ under pressure. *Solid State Commun.* **2005**, *136*, 262–267.
35. Nad, F.; Monceau, P.; Kaboub, L.; Fabre, J.M. Divergence of the relaxation time in the vicinity of the ferroelectric charge-ordered phase transition in $(\text{TMTTF})_2\text{AsF}_6$. *EPL* **2006**, *73*, 567–573.
36. Nad, F.; Monceau, P. Dielectric response of the charge ordered state in quasi-one-dimensional organic conductors. *J. Phys. Soc. Jpn.* **2006**, *75*, 1–12.
37. Hirose, S.; Kawamoto, A.; Matsunaga, N.; Nomura, K.; Yamamoto, K.; Yakushi, K. Reexamination of ^{13}C -NMR in $(\text{TMTTF})_2\text{AsF}_6$: Comparison with infrared spectroscopy. *Phys. Rev. B* **2010**, *81*, 205107.
38. Dressel, M.; Dumm, M.; Knoblauch, T.; Masino, M. Comprehensive optical investigations of charge order in organic chain compounds $(\text{TMTTF})_2\text{X}$. *Crystals* **2012**, *2*, 528–578.
39. Kitou, S.; Fujii, T.; Kawamoto, T.; Katayama, N.; Maki, S.; Nishibori, E.; Sugimoto, K.; Takata, M.; Nakamura, T.; Sawa, H. Successive dimensional transition in $(\text{TMTTF})_2\text{PF}_6$ revealed by synchrotron X-ray diffraction. *Phys. Rev. Lett.* **2017**, *119*, 065701.
40. Nogami, Y.; Nakamura, T. X-ray observation of $2k_F$ and $4k_F$ charge orderings in $(\text{TMTTF})_2\text{ReO}_4$ and $(\text{TMTTF})_2\text{SCN}$ associated with anion orderings. *J. Phys. IV* **2002**, *12*, 145–148.
41. Coulon, C.; Parkin, S.S.P.; Laversanne, R. Structureless transition and strong localization effects in bis-tetramethyltetrathiafulvalenium salts $[(\text{TMTTF})_2\text{X}]$. *Phys. Rev. B* **1985**, *31*, 3583–3587.
42. Yu, W.; Zhang, F.; Zamborszky, F.; Alavi, B.; Baur, A.; Merlic, C.A.; Brown, S.E. Electron-lattice coupling and broken symmetries of the molecular salt $(\text{TMTTF})_2\text{SbF}_6$. *Phys. Rev. B* **2004**, *70*, 121101.
43. De Souza, M.; Foury-Leylekian, P.; Moradpour, A.; Pouget, J.P.; Lang, M. Evidence for lattice effects at the charge-ordering transition in $(\text{TMTTF})_2\text{X}$. *Phys. Rev. Lett.* **2008**, *101*, 19–22.
44. De Souza, M.; Pouget, J.P. Charge-ordering transition in $(\text{TMTTF})_2\text{X}$ explored via dilatometry. *J. Phys. Condens. Matter* **2013**, *25*, 343201.
45. Foury-Leylekian, P.; Petit, S.; Andre, G.; Moradpour, A.; Pouget, J.P. Neutron scattering evidence for a lattice displacement at the charge ordering transition of $(\text{TMTTF})_2\text{PF}_6$. *Physica B* **2010**, *405*, 95–97.
46. Dumm, M.; Abaker, M.; Dressel, M. Mid-infrared response of charge-ordered quasi-1D organic conductors $(\text{TMTTF})_2\text{X}$. *J. Phys. IV (France)* **2005**, *131*, 55–58.
47. Dumm, M.; Abaker, M.; Dressel, M.; Montgomery, L.K. Charge Order in $(\text{TMTTF})_2\text{PF}_6$ Investigated by Infrared Spectroscopy. *J. Low Temp. Phys.* **2006**, *142*, 613–616.
48. Medjanik, K.; Chernenkaya, A.; Nepijko, S.A.; Ohrwall, G.; Foury-Leylekian, P.; Alemany, P.; Canadell, E.; Schonhense, G.; Pouget, J.P. Donor-anion interactions at the charge localization and charge ordering transitions of $(\text{TMTTF})_2\text{AsF}_6$ probed by NEXAFS. *Phys. Chem. Chem. Phys.* **2015**, *17*, 19202–19214.
49. Rose, E.; Loose, C.; Kortus, J.; Pashkin, A.; Kuntscher, C.A.; Ebbinghaus, S.G.; Hanfland, M.; Lissner, F.; Schleid, T.; Dressel, M. Pressure-dependent structural and electronic properties of quasi-one-dimensional $(\text{TMTTF})_2\text{PF}_6$. *J. Phys. Condens. Matter* **2013**, *25*, 014006.
50. Jacko, A.C.; Feldner, H.; Rose, E.; Lissner, F.; Dressel, M.; Valentí, R.; Jeschke, H.O. Electronic properties of Fabre charge-transfer salts under various temperature and pressure conditions. *Phys. Rev. B* **2013**, *87*, 155139.
51. Roobottom, H.K.; Jenkins, H.D.B.; Passmore, J.; Glasser, L. Thermochemical radii of complex ions. *J. Chem. Ed.* **1999**, *76*, 1570–1573.
52. Kaabel, S.; Adamson, J.; Topic, F.; Kiesila, A.; Kalenius, E.; Oeren, M.; Reimund, M.; Prigorchenko, E.; Lookene, A.; Reich, H.J.; et al. Chiral hemicucurbit[8]uril as an anion receptor: Selectivity to size, shape and charge distribution. *Chem. Sci.* **2017**, *8*, 2184–2190.

53. Oka, Y.; Matsunaga, N.; Nomura, K.; Kawamoto, A.; Yamamoto, K.; Yakushi, K. Charge order in (TMTTF)₂TaF₆ by infrared spectroscopy. *J. Phys. Soc. Jpn.* **2015**, *84*, 114709.
54. Nakamura, T.; Furukawa, K.; Hara, T. ¹³C NMR analyses of successive charge ordering in (TMTTF)₂ReO₄. *J. Phys. Soc. Jpn.* **2006**, *75*, 013707.
55. Matsunaga, N.; Hirose, S.; Shimohara, N.; Satoh, T.; Isome, T.; Yamamoto, M.; Liu, Y.; Kawamoto, A.; Nomura, K. Charge ordering and antiferromagnetism in (TMTTF)₂SbF₆. *Phys. Rev. B* **2013**, *87*, 144415.
56. Świetlik, R.; Barszcz, B.; Pustogow, A.; Dressel, M. Raman spectroscopy evidence of domain walls in the organic electronic ferroelectrics (TMTTF)₂X (X = SbF₆, AsF₆, PF₆). *Phys. Rev. B* **2017**, *95*, 085205.
57. Pouget, J.P.; Moret, R.; Comes, R.; Bechgaard, K.; Fabre, J.M.; Giral, L. X-Ray diffuse-scattering study of some (TMTSF)₂X and (TMTTF)₂X salts. *Mol. Cryst. Liq. Cryst.* **1982**, *79*, 129–143.
58. Nad, F.Y.; Monceau, P.; Carcel, C.; Fabre, J.M. Charge ordering in (TMTTF)₂X salts. *Synth. Met.* **2003**, *133*, 265–267.
59. Pouget, J.P.; Moret, R.; Comes, R.; Bechgaard, K. X-Ray diffuse scattering study of superstructure formation in tetramethyltetraselenafulvalenium perrhenate (TMTSF)₂ReO₄ and nitrate (TMTSF)₂NO₃. *J. Phys. Lett.* **1981**, *42*, doi:10.1051/jphyslet:019810042024054300.
60. Moret, R.; Pouget, J.P.; Comès, R.; Bechgaard, K. X-Ray scattering evidence for anion ordering and structural distortions in the low-temperature phase of di(tetramethyltetraselenafulvalenium) perrhenate [(TMTSF)₂ReO₄]. *Phys. Rev. Lett.* **1982**, *49*, 1008–1012.
61. Pouget, J.P.; Shirane, G.; Bechgaard, K.; Fabre, J.M. X-ray evidence of a structural phase transition in di-tetramethyltetraselenafulvalenium perchlorate [(TMTSF)₂ClO₄], pristine and slightly doped. *Phys. Rev. B* **1983**, *27*, 5203–5206.
62. Moret, R.; Ravy, S.; Pouget, J.P.; Comes, R.; Bechgaard, K. Anion-ordering phase diagram of di(tetramethyltetraselenafulvalenium) perrhenate, [(TMTSF)₂ReO₄]. *Phys. Rev. Lett.* **1986**, *57*, 1915–1918.
63. Coulon, C.; Delhaes, P.; Amiell, J.; Manceau, J.P.; Fabre, J.M.; Giral, L. Effect of doping (TMTSF)₂ClO₄ with TMTTF - I. Ambient pressure results : A competition between the different possible ground states. *J. Phys.* **1982**, *43*, 1721–1729.
64. Ilakovac, V.; Ravy, S.; Pouget, J.P.; Lenoir, C.; Boubekeur, K.; Batail, P.; Babic, S.D.; Biskup, N.; Korin-Hamzic, B.; Tomic, S.; et al. Enhanced charge localization in the organic alloys [(TMTSF)_{1-x}(TMTTF)_x]₂ReO₄. *Phys. Rev. B* **1994**, *50*, 7136–7139.
65. Tomic, S.; Auban-Senzier, P.; Jérôme, D. Charge localization in [(TMTTF)_{0.5}(TMTSF)_{0.5}]₂ReO₄: A pressure study. *Synth. Met.* **1999**, *103*, 2197–2198.
66. Tomić, S.; Jérôme, D.; Monod, P.; Bechgaard, K. EPR and electrical conductivity of the organic superconductor di-tetramethyltetraselenafulvalenium-perchlorate, (TMTSF)₂ClO₄ and a metastable magnetic state obtained by fast cooling. *J. Phys. Lett.* **1982**, *43*, 839–844.
67. Takahashi, T.; Jérôme, D.; Bechgaard, K. Observation of a magnetic state in the organic superconductor (TMTSF)₂ClO₄: Influence of the cooling rate. *J. Phys. Lett.* **1982**, *43*, 565–573.
68. Ishiguro, T.; Murata, K.; Kajimura, K.; Kinoshita, N.; Tokumoto, H.; Tokumoto, M.; Ukachi, T.; Anzai, H.; Saito, G. Superconductivity and metal-nonmetal transitions in (TMTSF)₂ClO₄. *J. Phys. Coll.* **1983**, *44*, C3-831–C3-838.
69. Yonezawa, S.; Marrache-Kikuchi, C.A.; Bechgaard, K.; Jérôme, D. Crossover from impurity-controlled to granular superconductivity in (TMTSF)₂ClO₄. *Phys. Rev. B* **2018**, *97*, 014521.
70. Parkin, S.S.P.; Mayerle, J.J.; Engler, E.M. Anion ordering in (TMTTF)₂ReO₄: A displacive transition. *J. Phys. Colloq.* **1983**, *44*, C3-1105.
71. Dumm, M.; Loidl, A.; Fravel, B.W.; Starkey, K.P.; Montgomery, L.K.; Dressel, M. Electron spin resonance studies on the organic linear-chain compounds (TMTCF)₂X (C = S, Se; X = PF₆, AsF₆, ClO₄, Br). *Phys. Rev. B* **2000**, *61*, 511–521.
72. Salameh, B.; Yasin, S.; Dumm, M.; Untereiner, G.; Montgomery, L.; Dressel, M. Spin dynamics of the organic linear chain compounds (TMTTF)₂X (X = SbF₆, AsF₆, BF₄, ReO₄, and SCN). *Phys. Rev. B* **2011**, *83*, 205126.
73. Coulon, C.; Foury-Leylekian, P.; Fabre, J.M.; Pouget, J.P. Electronic instabilities and irradiation effects in the (TMTTF)₂X series. *Eur. Phys. J. B* **2015**, *88*, 85.
74. Rohwer, A.; Dumm, M. Vibrational studies on TMTTF salts with non-centrosymmetric anions. To be published.
75. Nad, F.; Monceau, P.; Nakamura, T.; Furukawa, K. The effect of deuteration on the transition into a charge ordered state of (TMTTF)₂X salts. *J. Phys. Condens. Matter* **2005**, *17*, L399.

76. Furukawa, K.; Hara, T.; Nakamura, T. Deuteration effect and possible origin of the charge-ordering transition of (TMTTF)₂X. *J. Phys. Soc. Jpn.* **2005**, *74*, 3288–3294.
77. Pouget, J.P.; Foury-Leylekian, P.; Le Bolloc'h, D.; Hennion, B.; Ravy, S.; Coulon, C.; Cardoso, V.; Moradpour, A. Neutron-scattering evidence for a spin-Peierls ground state in (TMTTF)₂PF₆. *J. Low Temp. Phys.* **2006**, *142*, 147–152.
78. Jérôme, D.; Schulz, H. Organic conductors and superconductors. *Adv. Phys.* **1982**, *31*, 299–490.
79. Ishiguro, T.; Yamaji, K.; Saito, G. *Organic Superconductors*, 2nd ed.; Springer: Berlin, Germany, 1998.
80. Kagoshima, S.; Nagasawa, H.; Sambongi, T. *One-Dimensional Conductors*; Springer: Berlin, Germany, 1988.
81. Lebed, A. (Ed.) *The Physics of Organic Superconductors and Conductors*; Springer: Berlin, Germany, 2008.
82. Dumm, M.; Dressel, M.; Loidl, A.; Frawel, B.; Starkey, K.; Montgomery, L. Magnetic studies of (TMTTF)₂X (X=PF₆, ClO₄, and Br). *Synth. Met.* **1999**, *103*, 2068–2069.
83. Dumm, M.; Dressel, M.; Loidl, A.; Fravel, B.; Montgomery, L. Spin dynamics of organic linear chain compounds. *Physica B* **1999**, *259–261*, 1005–1006.
84. Lunkenheimer, P.; Loidl, A. Dielectric spectroscopy on organic charge-transfer salts. *J. Phys. Condens. Matter* **2015**, *27*, 373001.
85. Tomić, S.; Dressel, M. Ferroelectricity in molecular solids: A review of electrodynamic properties. *Rep. Prog. Phys.* **2015**, *78*, 096501.
86. Starešinić, D.; Biljaković, K.; Lunkenheimer, P.; Loidl, A. Slowing down of the relaxational dynamics at the ferroelectric phase transition in one-dimensional (TMTTF)₂AsF₆. *Solid State Commun.* **2006**, *137*, 241–245.
87. Brazovskii, S. Theory of the ferroelectric Mott-Hubbard phase in organic conductors. *J. Phys. IV* **2002**, *12*, 149–152.
88. Brazovskii, S. Ferroelectricity and charge-ordering in quasi-1d organic conductors. In *The Physics of Organic Superconductors and Conductors*; Lebed, A., Ed.; Springer: Berlin, Germany, 2008.
89. Brazovskii, S.; Monceau, P.; Nad, F.Y. Critical dynamics and domain motion from permittivity of the electronic ferroelectric (TMTTF)₂AsF₆. *Physica B* **2015**, *460*, 79–82.
90. Giovannetti, G.; Nourafkan, R.; Kotliar, G.; Capone, M. Correlation-driven electronic multiferroicity in (TMTTF)₂X organic crystals. *Phys. Rev. B* **2015**, *91*, 125130.
91. Brazovskii, S.; Monceau, P.; Nad, F. The ferroelectric Mott-Hubbard phase in organic conductors. *Synth. Met.* **2003**, *137*, 1331–1333.
92. Brazovskii, S. The theory for the ferroelectric Mott-Hubbard phase in organic conductors. *Synth. Met.* **2003**, *133–134*, 301–303.
93. Brazovskii, S. Theory of the ferroelectric phase in organic conductors: From physics of solitons to optics. *J. Phys. IV* **2004**, *114*, 9–13.
94. Lines, M.E.; Glass, A.M. *Principles and Applications of Ferroelectrics and Related Materials*; Clarendon Press: Oxford, UK, 1977.
95. Blinc, R. The soft mode concept and the history of ferroelectricity. *Ferroelectrics* **1987**, *74*, 301–303.
96. De Souza, M.; Squillante, L.; Sônego, C.; Menegasso, P.; Foury-Leylekian, P.; Pouget, J.P. Probing the ionic dielectric constant contribution in the ferroelectric phase of the Fabre salts. *Phys. Rev. B* **2018**, *97*, 045122.
97. Dressel, M.; Grüner, G. *Electrodynamics of Solids*; Cambridge University Press: Cambridge, UK, 2002.
98. Pinterić, M.; Ivek, T.; Čulo, M.; Milat, O.; Basletić, M.; Korin-Hamzić, B.; Tafra, E.; Hamzić, A.; Dressel, M.; Tomić, S. What is the origin of anomalous dielectric response in 2D organic dimer Mott insulators κ-(BEDT-TTF)₂Cu[N(CN)₂]Cl and κ-(BEDT-TTF)₂Cu₂(CN)₃. *Physica B* **2015**, *460*, 202–207.
99. Pinterić, M.; Čulo, M.; Milat, O.; Basletić, M.; Korin-Hamzić, B.; Tafra, E.; Hamzić, A.; Ivek, T.; Peterseim, T.; Miyagawa, K.; et al. Anisotropic charge dynamics in the quantum spin-liquid candidate κ-(BEDT-TTF)₂Cu₂(CN)₃. *Phys. Rev. B* **2014**, *90*, 195139.
100. Dressel, M.; Lazić, P.; Pustogow, A.; Zhukova, E.; Gorshunov, B.; Schlueter, J.A.; Milat, O.; Gumhalter, B.; Tomić, S. Lattice vibrations of the charge-transfer salt κ-(BEDT-TTF)₂Cu₂(CN)₃: Comprehensive explanation of the electrodynamic response in a spin-liquid compound. *Phys. Rev. B* **2016**, *93*, 081201.
101. Pinterić, M.; Lazić, P.; Pustogow, A.; Ivek, T.; Kuveždić, M.; Milat, O.; Gumhalter, B.; Basletić, M.; Čulo, M.; Korin-Hamzić, B.; Löhle, A.; et al. Anion effects on electronic structure and electrodynamic properties of the Mott insulator κ-(BEDT-TTF)₂Ag₂(CN)₃. *Phys. Rev. B* **2016**, *94*, 161105.
102. Ivek, T.; Korin-Hamzić, B.; Milat, O.; Tomić, S.; Clauss, C.; Drichko, N.; Schweitzer, D.; Dressel, M. Collective excitations in the charge-ordered phase of α-(BEDT-TTF)₂I₃. *Phys. Rev. Lett.* **2010**, *104*, 206406.

103. Ivek, T.; Korin-Hamzić, B.; Milat, O.; Tomić, S.; Clauss, C.; Drichko, N.; Schweitzer, D.; Dressel, M. Electrodynamic response of the charge ordering phase: Dielectric and optical studies of α -(BEDT-TTF)₂I₃. *Phys. Rev. B* **2011**, *83*, 165128.
104. Voloshenko, I.; Herter, M.; Beyer, R.; Pustogow, A.; Dressel, M. Pressure-dependent optical investigations of Fabre salts in the charge-ordered state. *J. Phys. Condens. Matter* **2017**, *29*, 115601.

Sample Availability: Samples of the (TMTTF)₂X compounds are available from the authors.



© 2018 by the authors. Licensee MDPI, Basel, Switzerland. This article is an open access article distributed under the terms and conditions of the Creative Commons Attribution (CC BY) license (<http://creativecommons.org/licenses/by/4.0/>).